Contents lists available at ScienceDirect

Bioactive Materials

Bioinspired multifunctional cellulose film: In situ bacterial capturing and killing for managing infected wounds

Chengcheng Li [a,*], Ya-Xuan Zhu [d], Ying Yang [a], Wanting Miao [a], Xiaotong Shi [a], Ke-Fei Xu [b], Zi-Heng Li [b], Huining Xiao [c,***], Fu-Gen Wu [b,**]

[a] *International Innovation Center for Forest Chemicals and Materials and Jiangsu Co-Innovation Center for Efficient Processing and Utilization of Forest Resources, Nanjing Forestry University, Nanjing, 210037, China*
[b] *State Key Laboratory of Digital Medical Engineering, Jiangsu Key Laboratory for Biomaterials and Devices, School of Biological Science and Medical Engineering, Southeast University, 2 Southeast University Road, Nanjing, 211189, China*
[c] *Department of Chemical Engineering, University of New Brunswick, Fredericton, New Brunswick, E3B 5A3, Canada*
[d] *Shanghai Frontiers Science Center of Nanocatalytic Medicine, Shanghai Tenth People's Hospital, School of Medicine, Tongji University, Shanghai, 200092, China*

A B S T R A C T

Bacterial infection of cutaneous wounds can easily lead to occurrence of chronic wounds and even more serious diseases. Therefore, multifunctional, biodegradable, and reusable wound dressings that can quickly manage wound infection and promote wound healing are urgently desired. Herein, inspired by the "capturing and killing" action of *Drosera peltata* Thunb., a biomimetic cellulose film was constructed to capture the bacteria (via the rough structure of the film) and kill them (via the combination of photodynamic therapy and chemotherapy) to promote wound tissue remodeling. The film (termed OBC-PR) was simply prepared by chemically crosslinking the oxidized bacterial cellulose (OBC) with polyhexamethylene guanidine hydrochloride (PHGH) and rose bengal (RB). Notably, it could effectively capture *Escherichia coli* and *Staphylococcus aureus* bacterial cells with capture efficiencies of ~99 % and ~96 %, respectively, within 10 min. Furthermore, the in vivo experiments showed that OBC-PR could effectively promote the macrophage polarization toward the M2 phenotype and adequately induce the reconstruction of blood vessels and nerves, thus promoting wound healing. This study provides a potential direction for designing multifunctional wound dressings for managing infected skin wounds in the future.

1. Introduction

Skin is the first defense line of human body against the external environments, and plays an important role in resisting the invasion of foreign pathogens [1]. Every year, many people suffer severe skin injury infections globally [2]. Bacterial infection brings great difficulties to wound healing and skin regeneration, and may lead to long-term chronic inflammation and cause serious diseases due to the excessive inflammatory responses, making it a serious global threat to human health and life [3,4]. Even worse, with the rapid increase of drug-resistant bacteria, especially the emergence of multidrug resistant bacteria, the development speed of new antibiotics is far behind [5–7], making the infected wound healing process more troublesome.

Currently, various efficient approaches, including supramolecular artificial receptor-modified macrophage (SAR-Macrophage) [8], chemo-dynamic therapy (CDT) [9–11], photothermal therapy [12,13], sonodynamic therapy [14], metal ion therapy [15], and photodynamic therapy (PDT) [16–18] or their combinations [19–21], have been applied for antiinfection purposes. However, these methods often do not have the function of wound healing promotion. Nature has greatly inspired us to develop new materials. In nature, *Drosera peltata* Thunb. can secrete glue to capture insects and kill them by secreting digestive fluid [22]. Two steps are involved in this process, including capturing and killing. Such a bioinspired action can provide new material design possibilities for developing new antibacterial materials to replace conventional antibiotics, which are prone to cause the occurrence of

drug-resistant bacteria. Designing such a bactericidal system, three conditions need to be considered. First, modules that can enhance the interaction of the fabricated material with bacteria must be integrated to allow the produced material to stick to the bacterial cells, and a large number of porous structures may be fabricated to increase the contact area of the material with bacteria, thus enabling the capture of more bacterial cells by the material. Second, an efficient and robust bactericidal system should be chosen to efficiently and quickly kill bacteria without using any antibiotics. Third, in consideration of sustainable development and ecological protection, the selected materials need to be safe, degradable, and reusable.
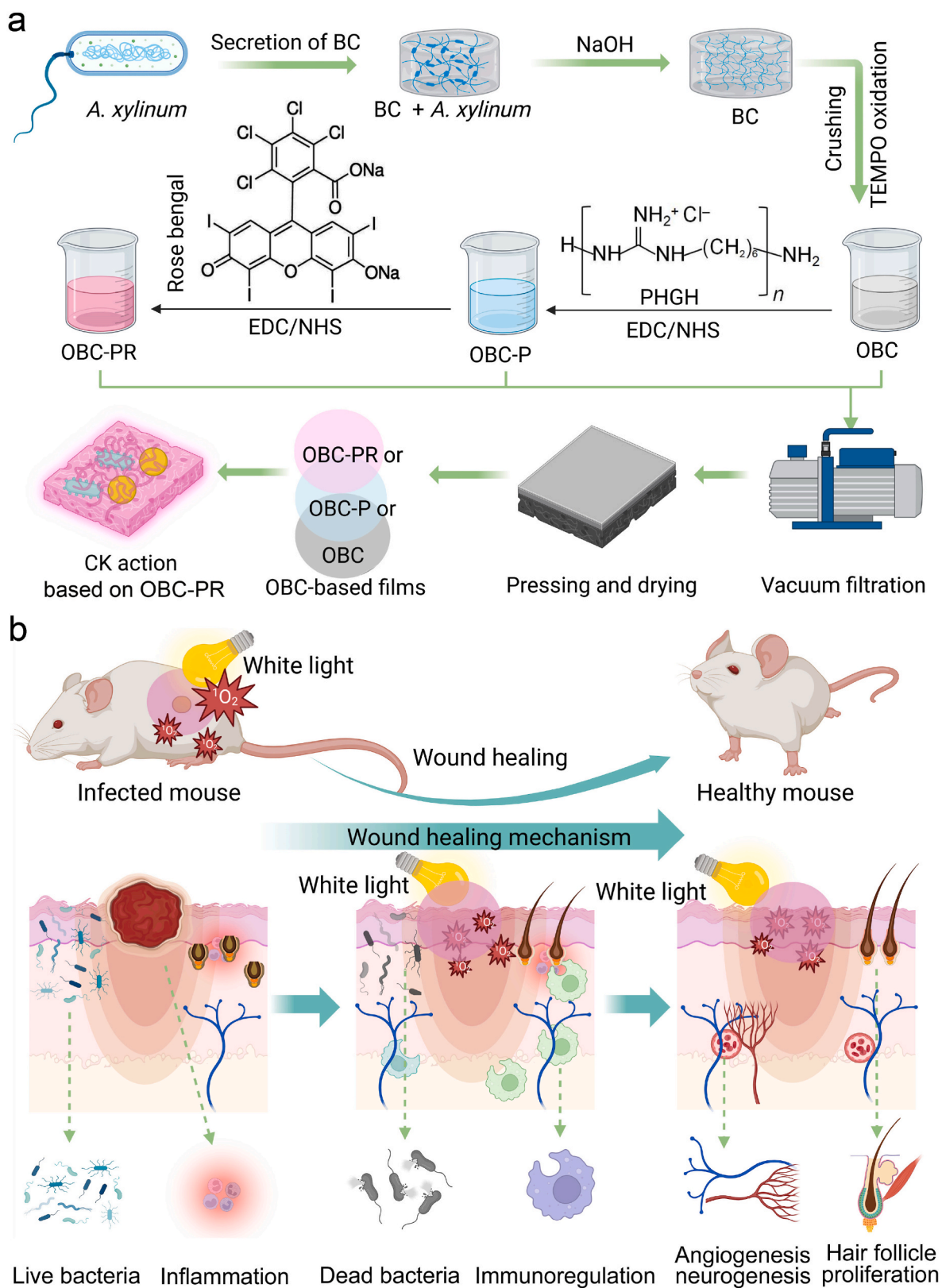
For skin repair and tissue regeneration, wound dressing represents an effective strategy [23]. Traditional wound dressings (gauze, cotton materials, etc.) only perform the simple functions of hemostasis and exudate absorption, and the traditional ones like cotton gauze bandages are easy to adhere to the wound, causing secondary damage [24]. More seriously, such dressings are prone to cause bacterial infection due to the absorption of wound extrudates in the mesh of the dressings [25]. To overcome these obstacles, a variety of materials have been developed as wound dressings, such as modified gauze [25], sponges [26,27], foams [28], and hydrogels [29]. Among these materials, hydrogels show unique application potential due to their three-dimensional (3D) network structure [30]. However, the stability and mechanical properties of traditional hydrogel materials are poor. In addition, traditional hydrogels often do not have the antibacterial properties, limiting their use in wound healing. Although many types of wound dressings have been developed, researchers and manufacturers mainly focus on the therapeutic effect of the wound dressings, but not on the biodegradability of wound dressings and their renewability after accomplishing certain tasks, causing widespread of the waste dressings in the environment and hence environmental burdens. Nowadays, developing new, environmentally friendly, and reusable wound dressing materials that can minimize the flow of hazardous waste into the environment while ensuring the product's functionality has become a critical issue. Besides, some additional requirements should be considered, such as the products after degradation should be non-toxic, and the degradation cycle should be controllable to meet different requirements. Therefore, it is crucial to develop an environmentally friendly and multifunctional dressing with simultaneous antiinflammatory, antibacterial, immunomodulation, and angiogenic abilities to effectively remodel the wound tissue and realize the rapid infected wound healing. Meanwhile, the safety and reusability of the degraded materials should be considered.

Bacterial cellulose (BC) is a natural nanofibrous polymer produced by bacteria, such as *Gluconacetobacter xylinus* (*G. xylinus*) [31]. BC exhibits some unique properties, including the 3D network structure, high water holding capacity, flexibility, high crystallinity, high purity, good mechanical properties, biodegradability after modification, excellent biocompatibility, and high permeability to liquids and gases [31]. All the above features make BC an ideal material for wound dressing. BC fibers are physically or chemically crosslinked to form a 3D hydrophilic network that absorbs a large amount of water (or biological liquids) and keeps the wound environment moist and cool, allowing oxygen to permeate through the network and promoting wound healing [32]. However, a simple BC dressing in its natural state usually needs to be functionalized to exert its antibacterial, antiinflammatory, immunomodulation, and angiogenic functions, and it has little effect on invasive pathogens and infected wounds [33]. Although BC can be functionalized with antibacterial agents or other functional substances to promote the infected wound healing [34,35], it only performs one or two functions, limiting their clinical applications. For example, Gutierrez et al. incorporated copper nanostructures in alginate/BC to obtain an antibacterial hydrogel by a 3D printing method [36]. Zhang et al. fabricated an Ag-pDA/BC (rGO) (pDA: polydopamine, rGO: reduced graphene oxide) film for wound dressing [37]. This composite film only possessed an additional antibacterial ability. Liu et al. constructed a TPEPy (pyridinium-substituted tetraphenylethylene)-grafted BC wound dressing by

in situ metabolizing TPEPy-modified glucose with *Komagataeibacter sucrofermentans* for skin wound repair [38]. However, this wound dressing accelerates the infected wound healing by killing the infected bacteria through the generation of reactive oxygen species (ROS) upon light irradiation, but it still lacks the function of immunoregulation. Therefore, developing multifunctional wound dressings for promoting infected wound healing is urgently needed.

PDT represents an effective strategy for fast antibacterial application without triggering bacterial drug resistance and can be used together with other antimicrobial modalities [39–41]. It employs various wavelengths of light to activate photosensitizers (PSs) in the presence of oxygen to generate ROS, mainly singlet oxygen, to destroy bacterial cell membrane and thereby release cellular inclusions for nonspecific antibacterial application, which only causes negligible drug resistance or no drug resistance of the bacteria [42]. PDT can also be integrated into various types of materials such as nanoplatforms [43], hydrogels [44], and films [45] to protect and enhance their efficacy [46]. Integration of PDT into porous materials is beneficial for improving the action efficiency due to the very small molecular weight of the produced ROS, which can quickly diffuse through the porous structure. However, PDT has some disadvantages in antibacterial application. For example, the lifetime of ROS generated by PSs is short (<200 ns), the interaction of bacteria with ROS is weak, and the diffusion distance of the produced ROS is very limited (about 20 nm), thereby only resulting in the damage to the bacteria immediately around it and restricting the wide application of PDT [47]. In addition, PDT fails to perform antibacterial activity when light illumination is removed, which may cause the recovery of bacteria and even the emergence of multidrug resistant bacteria [48]. ROS at high levels are effective in killing bacteria, but may cause oxidative stress, leading to serious pathological syndromes of patients, such as inflammation, necrosis, and fibrosis [48]. To solve the above problems of PDT, combination of PDT with other antibacterial strategies to satisfy the desire for effective antibacterial effect under both illumination and dark conditions may be feasible. Hu et al. incorporated berberine (BBR) and a living microalgae *Spirulina platensis* (SP) into carboxymethyl chitosan (CMCS) and sodium alginate (SA) to form a bioactive hydrogel (BBR@SP gel) as a multifunctional wound dressing [49]. Upon laser irradiation (650 nm), BBR could be constantly released from the BBR@SP gel, producing ROS to realize the combined chemo-photodynamic antibacterial therapy. Guanidine-based polymers showed excellent antimicrobial property by effectively disrupting the integrity of bacterial cells and penetrating into the biofilms and killing the bacterial cells in the biofilms, but are less toxic to human cells [50, 51]. Besides, such polymers are soluble in water, and their aqueous solutions are colorless, odorless, and non-corrosive [52]. Rose bengal (RB) is an anionic xanthene dye, possessing the photosensitive characteristic, and has been demonstrated to show a promising application potential in various biomedical fields [16,53]. RB exhibits intrinsic toxicity and selectivity towards different cancer cells [53] and microorganisms [16,53]. It has a good safety profile as a photodynamic agent with minimal potential side effects [53].

Inspired by the capturing and killing action of *Drosera peltata* Thunb. realized by secreting mucus substances, in this study, for the first time, we developed a biomimetic cellulose film that can interact effectively with bacterial cells, capture the bacterial cells by the rough cellulose-based materials, and then introduce PDT and chemotherapy modalities into this system to kill the captured bacteria. In detail, we fabricated a multifunctional polyhexamethylene guanidine hydrochloride (PHGH)- and RB-grafted BC (termed OBC-PR) film for fighting against bacterial infection and accelerating wound tissue remodeling by promoting the macrophage polarization toward the M2 phenotype and inducing the reconstruction of blood vessels and nerves, which in turn accelerated wound healing (Scheme 1). BC was first obtained by culturing *G. xylinus*, and then it was oxidized with 2,2,6,6-tetramethylpiperidine-1-oxyl (TEMPO) to obtain the BC with –COOH (termed OBC). Then, the obtained OBC was conjugated with PHGH or PHGH and rose bengal

Scheme 1. Design of OBC-based films and evaluation of their infected wound healing promotion effects. (a) Synthesis processes of OBC, OBC-P, and OBC-PR films and the CK action during the antibacterial process of the OBC-PR film. "CK" represents "C (capturing) and K (killing)". (b) Infected wound healing promoted by OBC-PR film and the related mechanisms.

through EDC•HCl (*N*-(3-dimethylaminopropyl)-*N'*-ethylcarbodiimide hydrochloride)/NHS (*N*-hydroxysuccinimide) chemistry to obtain the OBC-P and OBC-PR films with rough structure, good biocompatibility, and degradability. The rough network structure could trap bacteria and strengthened the capturing capacity possibly by forming hydrogen bonds between the protein/peptidoglycan of the exposed bacterial cells and the hydroxyl/amino/amide groups of the OBC-PR film. Subsequently, ROS were generated under white light irradiation around the bacterial cells, which were further rapidly killed by PHGH and the ROS released from RB in the film (Scheme 1). Under white light irradiation, the photodynamic effect of the OBC-PR film could also promote the infected wound healing. In addition, the OBC-PR film could create favorable immune microenvironment based on the antiinflammatory property of RB [54], suggesting its potential role as a wound repair material for infected wound healing. Moreover, the OBC-based films can be degraded by cellulase to fermentable sugars and then reused by *Acetobacter xylinum* (*A. xylinum*) to reproduce BC. Overall, the constructed biomimetic cellulose film has intelligent bacteria-capturing as well as antibacterial, antiinflammatory, immunomodulatory, and angiogenic abilities, and represents an efficacious strategy to achieve effective management of infected wound tissues.

2. Results and discussion

2.1. Synthesis and characterization of the OBC, OBC-P, and OBC-PR films

Fig. 1a shows the synthetic processes of various films based on BC, including OBC (oxidized BC), OBC-P (OBC conjugated with PHGH), and OBC-PR (OBC conjugated with PHGH and RB). The morphological structures of the films were first observed by field emission scanning electron microscopy (FESEM) and atomic force microscopy (AFM). All the films exhibited a 3D interweaved network structure, and the fiber diameters of the films were all around 26.0 nm (Fig. 1b). However, with increasing RB concentrations, we observed the appearance of some spherical structures in the OBC-PR films (Fig. S1). Such microspherical structure in the film may be due to the aggregation of RB by dye–dye interactions in the cellulose network structure [55]. To detect the distribution of RB in the OBC-PR film, the Raman mapping of the films was conducted. As shown in Fig. S2, the OBC-PR film showed obvious green and red colors, but not for the OBC and OBC-P films that do not contain RB, indicating that RB was uniformly distributed on the surface of the OBC-PR film. Fig. S3 displayed the corresponding electrostatic force microscopy (EFM) amplitude images of OBC, OBC-P, and OBC-PR films. When the tip voltage of 3 V was used, the color of the OBC-P film was
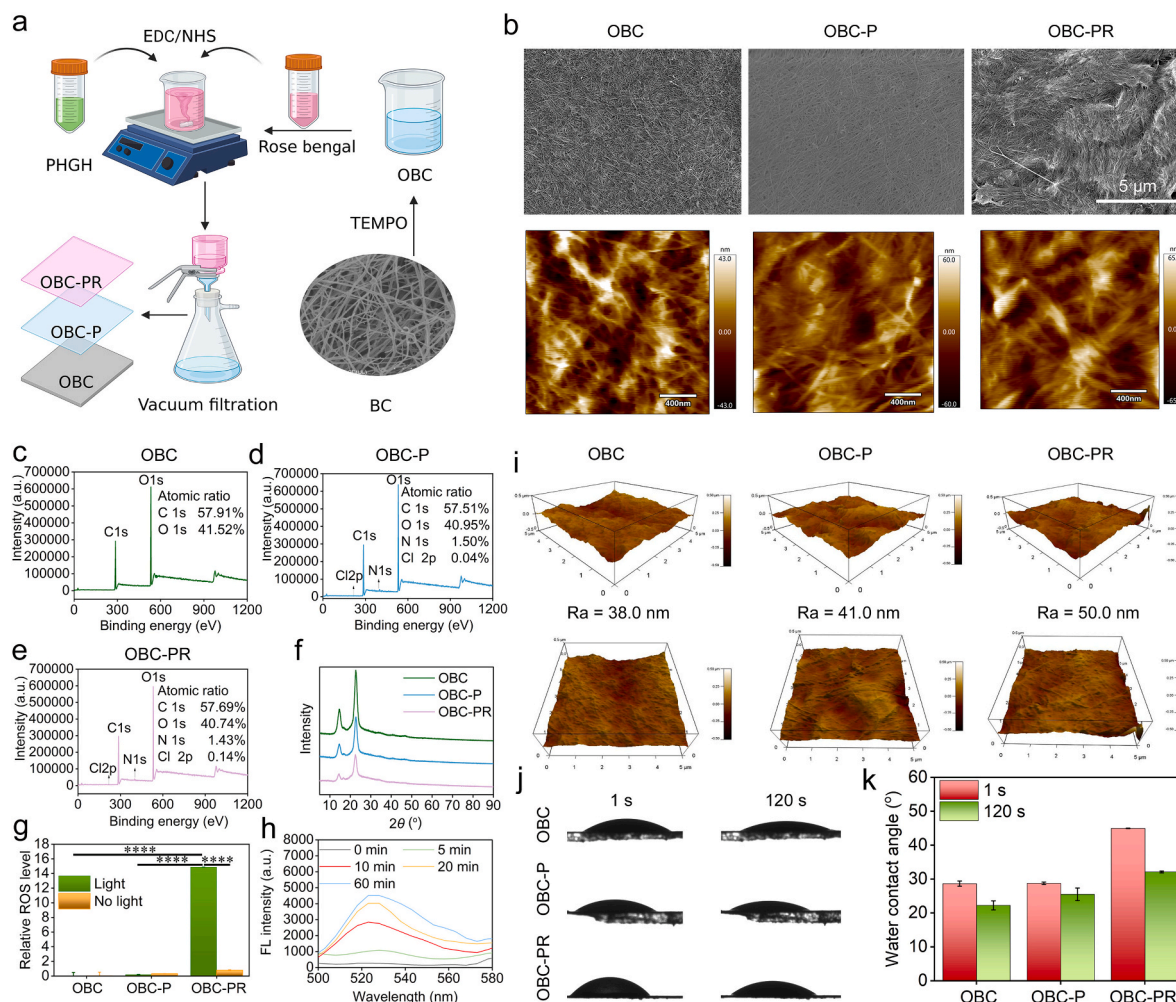

Fig. 1. Preparation processes and characterization of the OBC, OBC-P, and OBC-PR films. (a) Scheme showing the preparation steps of the films. (b) FESEM and AFM images of the films. (c–e) XPS patterns of the films. (f) XRD patterns of the films. (g) Relative ROS levels of the different films with or without light irradiation (10 min). (h) Fluorescence spectra of DCF after incubation of DCFH-DA with the OBC-PR film for different time periods. (i) 3D topographic AFM images of the films. Ra represents the average roughness. (j) Time-dependent water contact measurement results of the films. (k) Quantitative WCA results of the films at different contact time points. One-way analysis of variance (ANOVA) with Tukey's post-hoc test was used for statistical analysis. ****$P < 0.0001$.

obviously brighter than those of the other two films, meaning that a repulsive electrostatic force was generated in the OBC-P film while an attractive electrostatic force was observed in the other two films. Since PHGH is a positively charged polymer, the force between a positively biased tip and a positively charged polymer is obviously repulsive. However, RB is an anionic xanthene dye, which can interact with the biased tip, generating an attractive force. To identify the chemical compositions of the films, X-ray photoemission spectroscopy (XPS) was performed (Fig. 1c–e). The XPS total curve showed that OBC mainly contains C and O (Fig. 1c). Chlorine (Cl) is present in the XPS total curves of both OBC-P (Fig. 1d) and OBC-PR (Fig. 1e) with different amounts. The Cl in OBC-P indicated the successful conjugation of PHGH on OBC and the increased amount of Cl in OBC-PR indicated the successful conjugation of both PHGH and RB on OBC because both PHGH and RB contain Cl. Based on the inductively coupled plasma-mass spectrometry (ICP-MS) results, the RB content in OBC-PR was calculated to be 7 %. Furthermore, the X-ray diffraction (XRD) data (Fig. 1f) showed that similar characteristic peaks at $2\theta = 14.58°$ and $22.62°$ were observed in all the three films, indicating that the crystal structures of OBC-P and OBC-PR were similar to that of OBC. The ROS generation of the films with or without light irradiation was assessed with DCFH-DA (2′, 7′-dichlorodihydrofluorescein diacetate) as an ROS indicator. As shown in Fig. 1g, no fluorescence was detected for all the films without light irradiation. When the white light was applied to the films for 10 min, the characteristic 2′,7′-dichlorofluorescein (DCF) emission (at 525 nm) appeared in the OBC-PR group, indicating the production of ROS in this group. Furthermore, we evaluated the ROS production of the OBC-PR film after different irradiation time periods. As shown in Fig. 1h, the fluorescence intensity increased significantly with the increase of the irradiation time from 0 to 60 min. The fluorescence intensity of the OBC-PR group after irradiation for 60 min was ~17-fold that of the group without light irradiation. In addition, we also detected the production of $^1O_2$ by the OBC-PR film. As shown in Fig. S4, under light irradiation, OBC-PR produced $^1O_2$, which interacted with SOSG to produce fluorescence signals, and the fluorescence intensity was further enhanced when the irradiation time increased from 5 min to 90 min. Such a result indicated that OBC-PR can continuously generate $^1O_2$ to perform the long-time antibacterial action. All these results suggested that the OBC-PR film displays a strong ROS-producing ability and the ROS generation can last for a relatively long time period, which is beneficial for the long-term antibacterial application.

In addition, the surface morphology and characteristics, such as roughness and the hydrophilic/hydrophobic property are important factors that can affect the contact-killing efficiency of materials against pathogens [56,57]. Thus, the roughness of the OBC, OBC-P, and OBC-PR surfaces was first determined by AFM. The AFM height images of the surfaces of different films are shown in Fig. 1i and Fig. S5. The morphological structure of the film became rougher after modification with PHGH and RB, which was proved by the AFM results that the average roughness (Ra) value of OBC-PR film was ~1.3 times higher than that of the OBC film. With increasing RB concentrations, the Ra value of the films increased from 50 to 81 (Fig. S5) due to the presence of some spherical particles on the surface as shown in Fig. S1. Moreover, the surface roughness of a material can affect the material's surface wettability [58], further influencing the ability of bacteria to attach on or penetrate through the material, as well as the bacterial proliferation. Hence, wettability is quantified by the water contact angle (WCA) assay, and a surface is designated as hydrophilic when its WCA is lower than 90°. As shown in Fig. 1j and k, at the initial time point (1 s), the WCA values of OBC, OBC-P, and OBC-PR films were 28.7 ± 0.8°, 28.8 ± 0.4°, and 45.0 ± 0.1°, respectively, indicating the hydrophilicity of the films. In addition, the WCA values of the films were all lower than 90° within the detected time period (120 s); however, the WCA value of the OBC-PR film was higher than that of the OBC and OBC-P films. It has been reported that although hydrophilic dressings like gauze can quickly absorb fluid from the wound site, they can also cause some serious side effects

such as the growth of newborn granulation tissue into the mesh of the gauze, leading to secondary wound injury [59]. The WCA values of moderately wettable materials for protein adsorption and cell adhesion are in the range of 40–60° [60]. Therefore, the relatively higher WCA value of the OBC-PR film indicated its relatively hydrophobic surface, which is beneficial for the film to capture bacterial cells. Thus, the OBC-PR film may have better protein adsorption and cell attachment performance compared with other films.

2.2. Mechanical and water holding properties of the OBC, OBC-P, and OBC-PR films

As shown in Fig. 2a, the thicknesses of the obtained films showed a small difference. The OBC film was the thinnest one with the thickness of 16.8 μm. The thicknesses of OBC-P and OBC-PR increased to 18.0 and 20.3 μm, respectively. The increased thicknesses of the OBC-P and OBC-PR films were mainly due to the incorporation of PHGH and RB. In addition, the water retention ability of a film helps maintain the moisture of the wound microenvironment, accelerating wound healing [61]. We therefore detected the water retention ability of the films. As shown in Fig. 2b, the water retention ratio of the three types of films decreased with time. Among the three kinds of films, the OBC film displayed the fastest water loss rate, showing a water content of 43 % after 24 h treatment. However, the OBC-PR film showed the slowest water loss rate with a water content of 72 % after 24 h treatment, indicating that the OBC-PR film could keep moist for about 24 h, providing a mild environment for tissue regeneration in the wound area. Further, we detected the mechanical properties of the films. As shown in Fig. 2c, the tensile stress of the OBC, OBC-P, and OBC-PR films increased with the increase of the strain and then sharply decreased. The peak of the tensile strength of the OBC-PR film was 74.4 MPa, which was 4.92- and 1.90-fold that of the OBC (15.12 MPa) and OBC-P (39.17 MPa) films, respectively. In addition, based on the stress–strain curves (obtained by tensile strength measurements) and the frequency, amplitude, and phase of the viscoelastic mode of the AFM results, the Young's modulus values of the films were also calculated. As shown in Fig. 2d and S6, the OBC film showed the highest Young's modulus value and the OBC-P and OBC-PR films exhibited decreased Young's modulus values, indicating that the conjugation of PHGH or PHGH/RB onto the surface of the OBC film reduced the Young's modulus of the OBC film. However, the Young's modulus values of OBC-P and OBC-PR films were 54.8 and 70.0 MPa (as measured by tensile strength measurements) (Fig. 2d), respectively, which are much higher than that of the human skin (0.02–18 MPa) [62].

Subsequently, we investigated the microstructures of the films by FESEM. As displayed in the cross-section results in Fig. 2e, all the films were composed of multilayer cellulose with porous structures, exhibiting highly ordered lamellar microstructure. The layer number in the OBC-P and OBC-PR films was much higher than that in the OBC film, which may be beneficial for the OBC-P and OBC-PR films to trap bacterial cells. Furthermore, the high-magnification SEM images of OBC, OBC-P, and OBC-PR films showed the different cross-sectional lamellar structures. The number of the porous structure in OBC-P and OBC-PR films increased and the size of the pore became smaller. The increased pore number raised the specific surface area of the films, which may enhance the capturing capacity of the films against bacterial cells. In addition, the cross-section results showed that the gaps of OBC-PR film were wider than that of OBC film, indicating that the OBC-PR film was looser. This characteristic may be beneficial to the outstanding flexibility of the film. Moreover, no fracture was observed even if the OBC-PR film was folded into a desired shape (Fig. S7).

To verify that the OBC-PR film was suitable for dynamic wound healing process and easy to use, we adhered the films that were wetted before use to the finger joints, and then the films were twisted and photographed (Fig. 2f and g). The results showed that all the films could attach to the finger joints, and when the finger bent to different degrees, the films could still adhere to the finger, showing good adhesive
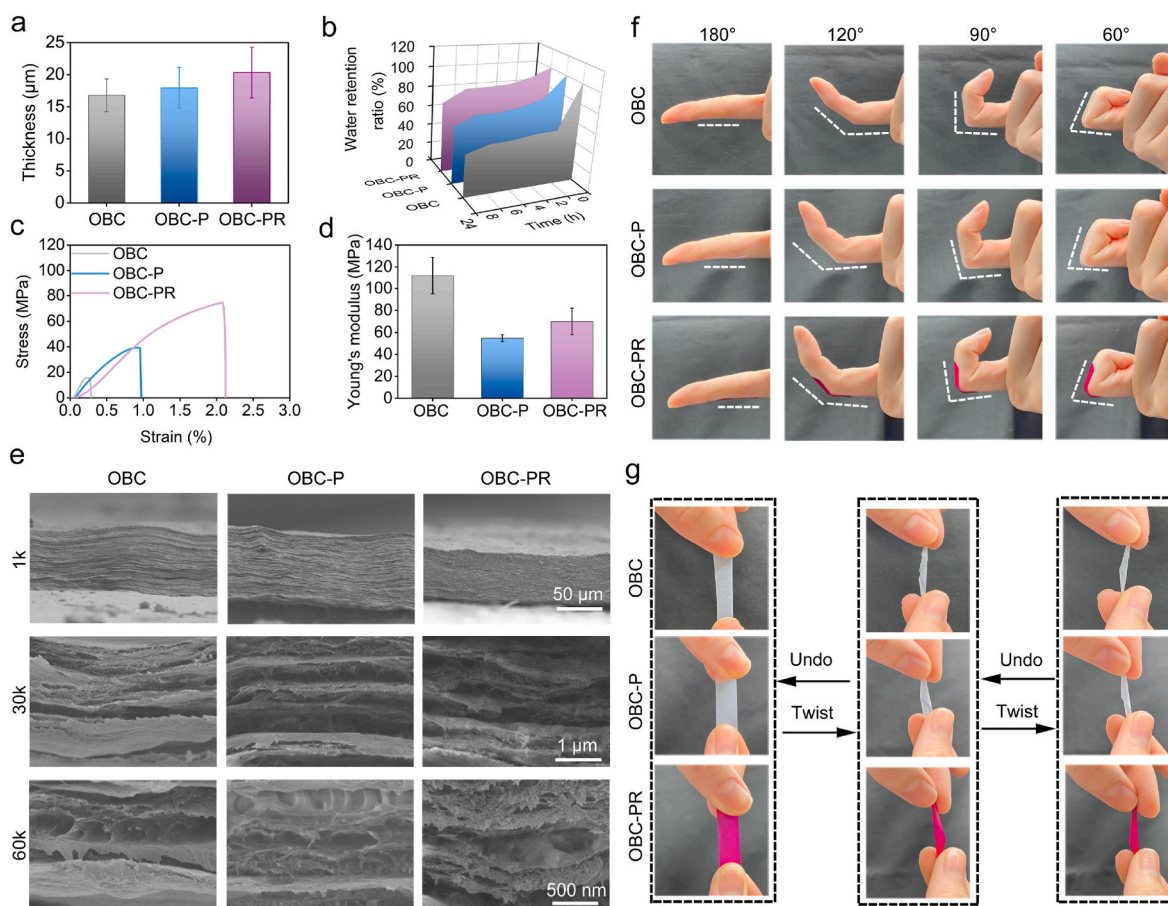
Fig. 2. Investigation on the mechanical properties of OBC, OBC-P, and OBC-PR films. (a) Thickness values of the films. (b) Water retention ratios of the films at 37 °C. (c) Stress–strain curves of the films. (d) Young's modulus values of the films. (e) Cross-section FESEM images of the films at different magnifications (1k, 30k, and 60k). (f) Photographs showing the attachment of the films after adsorbing water on human finger joints during exercise. (g) Photographs showing the films before and after twisting.

property, which was beneficial for their application as adhesive dressings to treat dynamic wounds by enhancing the connections between dynamic wounds and dressings. Moreover, the films were not ruptured after twisting, displaying that the films possess good flexibility under extreme environments (Fig. 2g). All these results confirmed the application potential of the OBC-P and OBC-PR films as wound dressings.

2.3. Bacterial capture performance of OBC, OBC-P, and OBC-PR films

A surface's properties like charge, hydrophobicity/hydrophilicity, and roughness will affect its bacterial entrapment and antibacterial abilities [63]. Considering the unique properties (e.g., moderate hydrophilicity and rough surface) of the OBC-PR film, we further evaluated its bacterial capture ability against Gram-negative *Escherichia coli* (*E. coli*) and Gram-positive *Staphylococcus aureus* (*S. aureus*) cells in vitro by environmental scanning electron microscopy (ESEM) and 3D confocal microscopic observation. As shown in Fig. 3a, the most bacteria including *S. aureus* and *E. coli* were located on the OBC-PR film, the number of bacteria on the OBC-P film was the second, and only a few bacteria were found on the OBC film, indicating that the OBC-PR film exhibited a strong ability to capture bacteria (both *E. coli* and *S. aureus*). The 3D confocal images shown in Fig. 3b further supported the above result. As displayed in the figure, after incubation of the bacteria with the films for 10 min, a large number of the SYTO 9-stained bacteria (green) appeared in the OBC-PR film for both *E. coli* and *S. aureus*. The fluorescence of the SYTO 9-stained bacteria in the OBC-P group was stronger than that of the OBC group and a little weaker than that of the OBC-PR group. Moreover, it could be seen that the fluorescence of the

SYTO 9-stained bacteria on the OBC film was weak, and the distribution of the fluorescence was more even, while the intensity of the fluorescence on the OBC-PR film was much higher and more concentrated, indicating that the OBC-PR film had a strong ability to capture bacteria. All the above data indicated that compared with a flat surface, the rough surface of OBC-PR film could increase the material's contact area with bacteria and specifically capture the bacteria to make the bacterial cells contact the RB of the OBC-PR film, allowing effective contact of ROS with the bacteria when the film was light irradiated to kill the bacteria efficiently. To further reveal the fast capturing effect of the OBC-PR film compared with the other two types of OBC-based films, we subsequently investigated the capture efficiency of the OBC, OBC-P, or OBC-PR film toward *E. coli* or *S. aureus*. As shown in Fig. 3c, the number of the bacterial colonies formed from the bacterial suspensions (with the OBC-PR films removed) both decreased after the incubation of the bacterial cells with the OBC-PR films, suggesting that the film can efficiently remove the bacterial cells from the bacterial suspensions. The bacterial capture efficiencies of the OBC-PR film reached 98.96 % and 96.17 % for *E. coli* and *S. aureus* cells, respectively (Fig. 3d), demonstrating that the film possesses an excellent bacterial capture ability. The OBC-P film showed moderate capture efficiencies for *E. coli* (67.63 %) and *S. aureus* (34.83 %) cells, but lower than those of the OBC-PR film. Among all the three types of OBC-based films, the capture efficiencies of the OBC film for *E. coli* (57.63 %) and *S. aureus* (24.83 %) were the lowest. Such difference in the bacterial capture efficiency of the films may be due to the different surface roughness and the charge variation contributed by RB. In summary, we developed a bioinspired material that imitates the capturing and killing process of *Drosera peltata* Thunb. toward insects to perform a
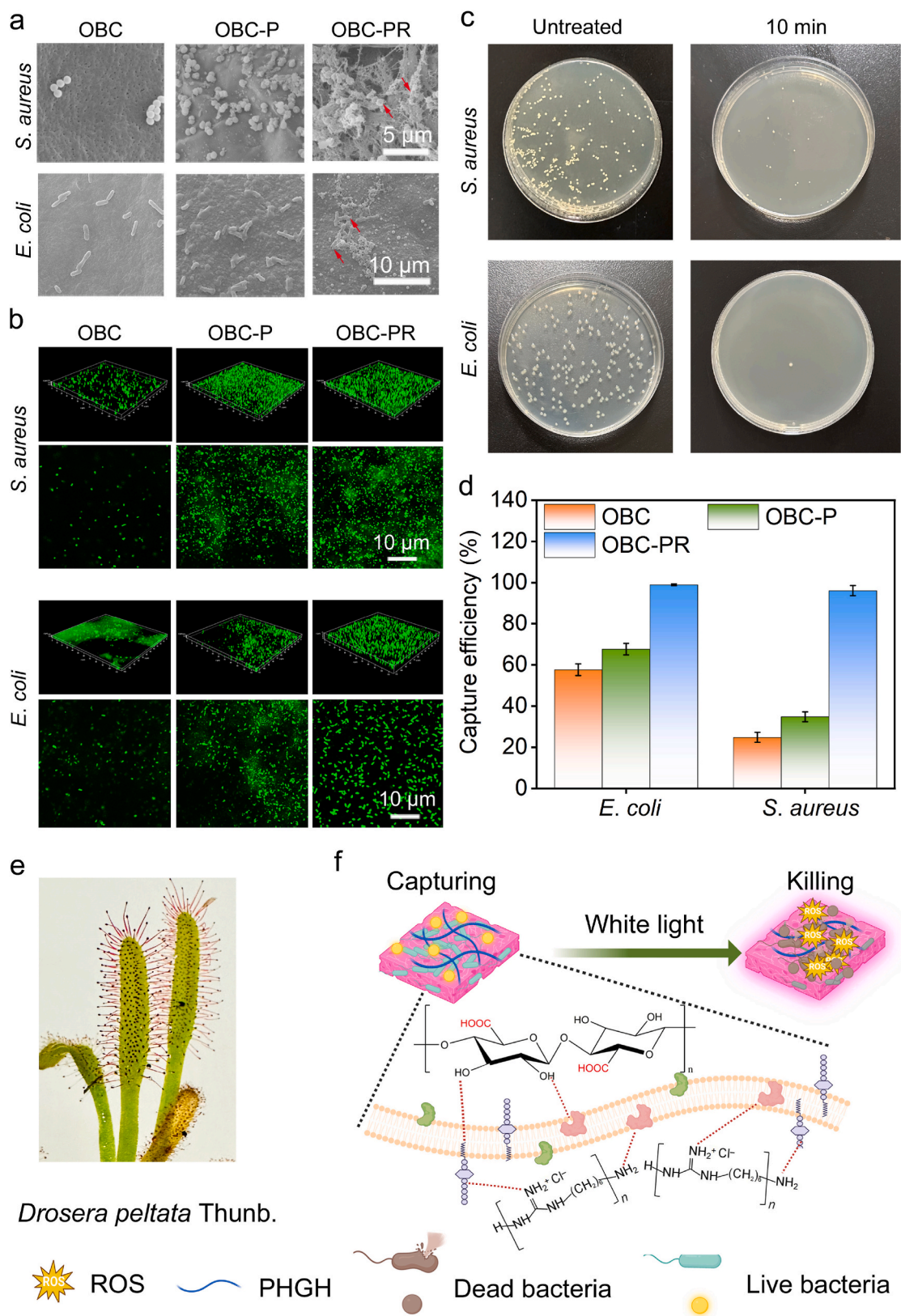
Fig. 3. In vitro evaluation of the bacteria-capturing abilities of OBC, OBC-P, and OBC-PR films. (a) ESEM images showing the *S. aureus* and *E. coli* bacterial cells attached on the films after 10 min incubation. (b) 3D confocal images of the SYTO 9-stained bacterial cells on the films after incubation with the films for 10 min. (c) Photographs showing the bacterial colonies formed on the agar plates. The bacterial colonies were formed by the untreated *S. aureus* and *E. coli* cells and the residual *S. aureus* and *E. coli* cells in the supernatants of the bacterial suspensions obtained by mixing 10^6 CFU/mL of *S. aureus* and *E. coli* cells with the OBC-PR film for 10 min. (d) Capture efficiencies of the OBC, OBC-P, and OBC-PR films toward *S. aureus* and *E. coli* cells. (e) Image of *Drosera peltata* Thunb. (f) Scheme illustrating the "ECK" action of OBC-PR film toward *S. aureus* and *E. coli* cells.

CK (C: capturing, K: killing) action for antibacterial application (Fig. 3e and f). The OBC-PR film exhibited excellent bacterial capture ability within a very short contact time (10 min), showing a great potential as an antibacterial wound dressing for treating infected wounds through two steps (Fig. 3f): 1) capturing bacterial cells through its rough structure possibly via the hydrogen bond formation between the film and the bacterial cell surface and 2) killing the captured bacterial cells by PHGH and ROS produced in the film under light illumination.

2.4. In vitro antibacterial performance of OBC, OBC-P, and OBC-PR films

Based on the excellent bacteria-capturing ability and the strong ROS-producing capacity of the OBC-PR film, we subsequently evaluated the in vitro antibacterial ability of the OBC, OBC-P, and OBC-PR films against Gram-positive *S. aureus* and Gram-negative *E. coli* cells by the colony counting method. The OBC, OBC-P, and OBC-PR films with a size of 1×1 cm were put into a 24-well plate and 200 μL of the bacterial cell suspension at an OD_{600} (optical density at 600 nm) of 0.5 was added onto the surface of the films, and treated with or without white light irradiation for different time periods. As shown in Fig. 4a and b and Fig. S8, the OBC group showed an almost unchanged survival bacterial fraction on the lysogeny broth (LB) agar plates with or without light irradiation at any time point, indicating that no antibacterial effect was observed for the OBC film against both *E. coli* and *S. aureus*. In the OBC-P

group, it could be seen that the number of both *E. coli* and *S. aureus* cells decreased compared with the OBC group under the light irradiation condition (Fig. 4a). OBC-based films have very different effects on Gram-negative and Gram-positive bacteria, as the two types of bacteria possess different cell-surface structures, leading to different resistance to ROS [64]. Specifically, the outer membrane of Gram-negative bacteria can protect the bacteria from the influence of extracellular ROS and make them less sensitive to ROS; however, Gram-positive bacteria lack an outer membrane, making them more sensitive to ROS [65,66]. In the dark condition, as shown in Fig. S8, the bacterial survival rates in the OBC-P and OBC-PR groups were very similar at all the tested time points (except for the 5-min results for *S. aureus*) for both types of bacteria, suggesting that RB does not play a noticeable antibacterial role; however, the bacterial survival rates in the OBC-P and OBC-PR groups were both lower than those in the OBC group for both types of bacteria, demonstrating that the antibacterial ability of OBC-P was mainly from PHGH. Besides, the bacterial survival rates in the OBC-P and OBC-PR groups also decreased with increasing incubation time. Specifically, after incubation for 20 min, the survival rates of *S. aureus* and *E. coli* cells were $\sim1.4 \times 10^{-6}$ and $\sim1.0/1.5 \times 10^{-7}$, respectively (for OBC-PR and OBC-P). These results suggested that the OBC-P and OBC-PR films were both robust antibacterial materials. Under light irradiation, as shown in Fig. 4a and b, the survival rates of *S. aureus* and *E. coli* both decreased significantly with increasing irradiation time from 5 to 30 min in the OBC-PR group, which was consistent with the ROS production results as
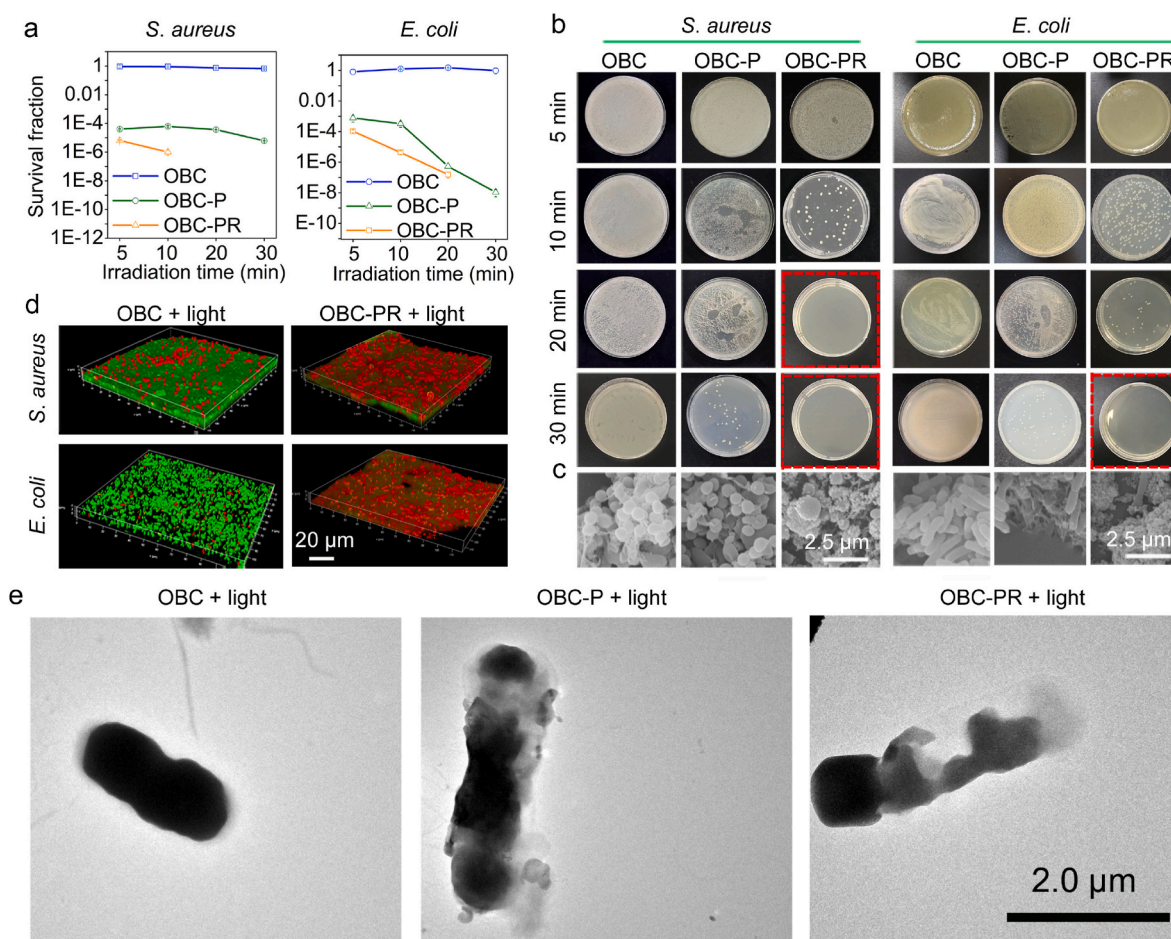

Fig. 4. In vitro evaluation of the antibacterial activities of OBC, OBC-P, and OBC-PR films with light irradiation. (a) Survival fractions of *S. aureus* and *E. coli* bacteria that were separately incubated with different films and irradiated by light for different time periods. (b) Photographs showing the agar plates of the *S. aureus* and *E. coli* cells that were treated separately with different films and irradiated by light for different time periods as indicated. Note that the images marked with red box did not have any bacterial cells. (c) ESEM images showing the *S. aureus* and *E. coli* cells after incubation with different films under white light irradiation for 15 min. (d) 3D confocal images of the SYTO 9- and PI-stained bacterial cells after exposure to different films under white light irradiation for 20 min. (e) TEM results of the *E. coli* cells treated by the OBC-PR film and irradiated by light for 15 min.

shown in Fig. 1h. Especially, after irradiation for 20 min (for *S. aureus*) and 30 min (for *E. coli*), the bacteria were completely killed, demonstrating that light irradiation could elevate the antibacterial efficacy of OBC-PR. In addition, the illumination time for completely killing the *E. coli* cells of OBC-PR film was longer than that for completely killing *S. aureus*. Such different antibacterial effects of the film toward the two types of bacteria were due to their different cell wall structures. Gram-negative bacteria possess an outer membrane composed of phospholipids and lipopolysaccharides (LPS), which can prevent various drugs from passing through the cell wall, thus weakening their antibacterial effects [67,68].

Subsequently, we tried to increase the loading content of RB in the OBC-PR film to improve the antibacterial activity of the films. However, the antibacterial activity of the OBC-PR film with a higher content of RB decreased significantly (Fig. S9), which may be because that the aggregation of RB molecules within the films can decrease the production of singlet oxygen upon light irradiation, thus lowering the antibacterial activity of the OBC-PR film [55]. Moreover, as shown in Fig. S10, the high antibacterial activities of OBC-P and OBC-PR against *E. coli* and *S. aureus* could last for a long time period (60 days). By contrast, the OBC film quickly became seriously contaminated as reflected by the bacterial growth around and on the OBC film (Fig. S10). The remarkable antibacterial performance of the OBC-PR film may be because that after the OBC-PR film captured the bacteria, the bacteria were placed in a microenvironment with high local concentrations of PHGH and RB, thereby persistently and then synergistically killing the bacteria by the action of PHGH and the produced ROS. The above results indicated that the capture ability of the OBC-PR film and the synergistic effects of PHGH and RB play important roles in elevating the antibacterial rate and shortening the antibacterial time, which could be helpful for controlling the infections in the wound area.

To further investigate the antibacterial mechanism of the OBC-P and OBC-PR films, FESEM assay and live/dead staining were conducted. It could be seen from Fig. 4c that the surfaces of *S. aureus* and *E. coli* in the OBC + light group were smooth and the structures of the bacterial cells were intact, indicating that OBC had no obvious damaging effect to the bacterial cells. In the OBC-P + light group, the bacterial cells were deformed and collapsed with a wrinkled morphology. More importantly, when OBC-PR together with light irradiation was applied to treat the bacterial cells, the cell surfaces of both *S. aureus* and *E. coli* manifested much more serious damage and collapse compared with that treated with the OBC film plus light irradiation, confirming the strongest antibacterial activity of OBC-PR owing to its synergistic PDT and chemotherapy effect. The FESEM results revealed that OBC-P and OBC-PR effectively killed bacteria via destroying the cell surface structure under light irradiation. Confocal laser scanning microscopy (CLSM) plus live/dead cell staining was then adopted to observe the cell membrane integrity of *S. aureus* and *E. coli* cells after various treatments. As shown in Fig. 4d, for both *S. aureus* and *E. coli*, the bacteria were almost all red due to the entrance of the propidium iodide (PI) dye through the compromised cell surface after the OBC-PR + light treatment, indicating the strong damaging effect of OBC-PR on the bacterial membrane. However, for the OBC + light group, most bacteria were stained green, indicating that these bacteria were alive. Such an antibacterial mechanism by destroying the cell surface makes it difficult for bacteria to develop drug resistance. Furthermore, transmission electron microscopy (TEM) imaging was conducted to display more detailed information on bacterial membrane damage. As shown in Fig. 4e, the *E. coli* cells treated with the OBC film and light irradiation were intact with regular rod-shaped structures. However, when OBC-P or OBC-PR plus light irradiation was used to treat *E. coli* cells, the cell surfaces of *E. coli* were severely damaged and the inner structures were also disrupted. The introduction of RB further enhanced the disruption ability of the OBC-P film to bacterial cells due to the production of ROS around the bacterial cells under the light irradiation condition. These results demonstrated that cell surface disruption was one of the antibacterial mechanisms for

the OBC-PR film.

All the above results and analyses enabled us to well illustrate the antibacterial mechanism of the films. First, the bacterial cells are trapped on the OBC-P or OBC-PR film. Then, the PHGH and the ROS generated by the OBC-PR film upon light irradiation destroy the cell surface structure by destabilizing and oxidizing the cell wall/membrane. Finally, the bacteria are killed by the synergistic action of PHGH and ROS. More importantly, the bacterial killing time is comparable to or shorter than that of other antibacterial materials as shown in Table S1.

2.5. Inhibition of biofilm growth by the OBC-P and OBC-PR films

Encouraged by the excellent antibacterial activity of the OBC-PR film against the planktonic bacteria, we proposed that the OBC-PR film may also inhibit the formation of biofilms due to the excellent bacterial killing and the long-time bacterial inhibition ability as shown in Fig. 4 and Fig. S10. We thus conducted the biofilm inhibition experiments. The *E. coli* and *S. aureus* suspensions were first cocultured with OBC, OBC-P, or OBC-PR film in 96-well plates under dark or light conditions for 20 min at 28 °C. Then, the films were removed from the bacterial suspensions, which were further incubated at 28 °C for 24 h. Afterward, the adhered biofilms after different treatments were stained with crystal violet (CV) and the biomass was quantified by detecting the absorbance of the samples at 590 nm. As displayed in Fig. 5a and d, the OBC-P- and OBC-PR-treated groups were light purple in color, while the control and OBC-treated groups showed dark purple in color, indicating that the OBC-P and OBC-PR could significantly inhibit the adherence of the bacterial cells onto the surface of the 96-well plates due to the inactivation of bacterial cells under both dark and light irradiation conditions, thus inhibiting the formation of biofilms. The quantification results also showed that the biofilms were significantly inhibited in the OBC-P- and OBC-PR-treated groups under both dark and light irradiation conditions for both *E. coli* and *S. aureus* (Fig. 5b and e). Subsequently, live/dead staining with the SYTO 9/PI dye was conducted to further evaluate the antibiofilm ability of the films against the biofilms formed by *E. coli* and *S. aureus* after different treatments and the treated biofilms after staining were observed with CLSM. As shown in Fig. 5c and f, the biofilms formed by *E. coli* and *S. aureus* in the OBC groups with or without light irradiation showed dense structures and displayed massive green fluorescence, accompanied with much less red fluorescence, indicating that the bacteria in the OBC groups successfully formed biofilms and the bacteria in the biofilms were mostly alive. However, when the *E. coli* bacteria were pretreated with OBC-P with or without light irradiation for 20 min, their capacity to form biofilms was weakened. Additionally, when the *E. coli* and *S. aureus* bacteria were pretreated with OBC-PR with or without light irradiation for 20 min, the biofilms formed by both bacteria were sharply decreased and most bacteria remained were dead.

2.6. In vivo infected wound healing promotion by the OBC, OBC-P, and OPC-PR films

After evaluating the inhibition effects of the different films on biofilm growth, we assessed their in vivo antibacterial abilities and wound healing promotion effects toward the *S. aureus*-infected wounds in mouse models. The whole in vivo experimental process is illustrated in Fig. 6a. After 1 day's infection with 100 μL of *S. aureus* suspension ($OD_{600} = 0.5$), the mice were randomly divided into 6 groups, including (1) OBC + light, (2) OBC-P + light, (3) OBC-PR + light, (4) OBC, (5) OBC-P, and (6) OBC-PR. The groups 1, 2, and 3 were irradiated with white light (4.5 mW/cm^2) for 10 min. The groups 4, 5, and 6 were stayed in the dark for 10 min. Wound photographs were taken on day 1, 3, 5, 9, and 11 to assess the wound healing promotion abilities of different films. As shown in Fig. 6b–d, the wound size of each group was reduced to some extent on the 9th day. The relative wound sizes in the OBC-P + light and OBC-PR + light groups reduced to (45.3 ± 3.1)% and (39.1 ± 1.4)%, which were smaller than that of the OBC + light group ((68.0 ±
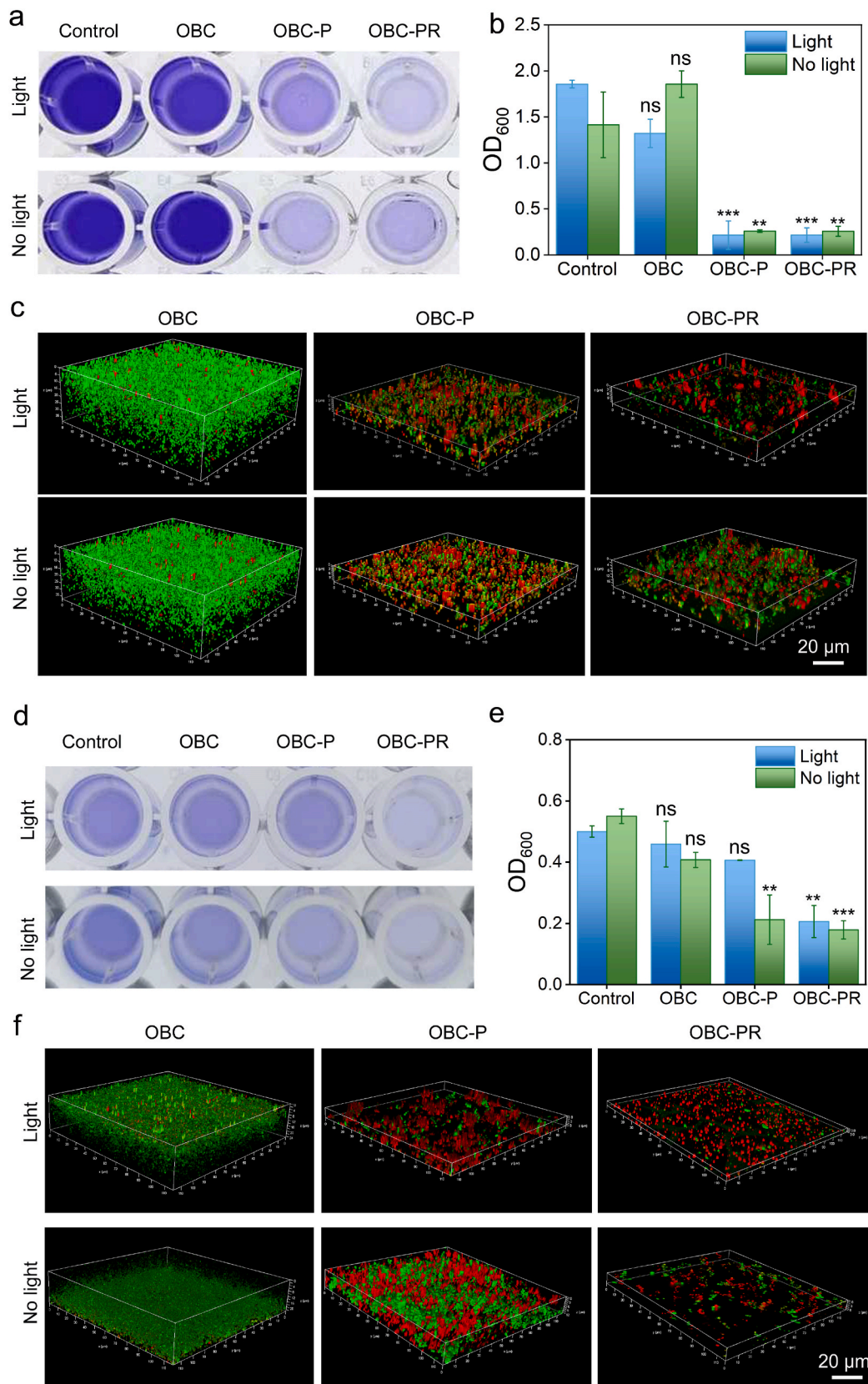
Fig. 5. Biofilm inhibition evaluation of OBC, OBC-P, and OBC-PR films. (a,d) Photographs of CV-stained *E. coli* (a) and *S. aureus* (d) biofilms after different treatments as indicated. Control: the biofilms without film treatment. (b,e) Biomass values (based on OD_{600} values) of the *E. coli* (b) and *S. aureus* (e) biofilms after treatment with different films for 24 h. Control: the biofilms without film treatment. (c,f) 3D confocal images of the biofilms formed by *E. coli* (c) and *S. aureus* (f) after different treatments as indicated. ANOVA with Tukey's post-hoc test was used for the significance analysis between multiple groups. ns, non-significance, **$P < 0.01$, ***$P < 0.001$ for the OBC, OBC-P, and OBC-PR groups versus the respective control groups.
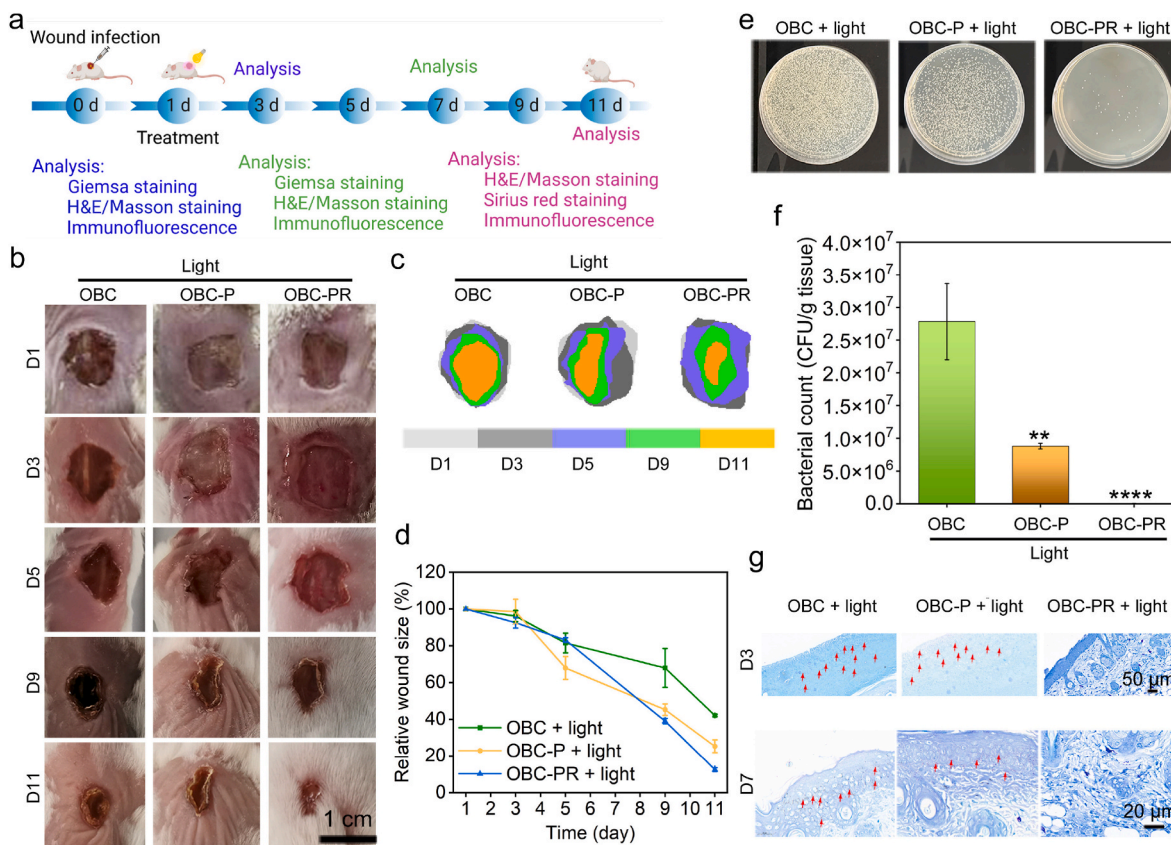
Fig. 6. In vivo infected wound healing promotion effects of OBC, OBC-P, and OBC-PR films (plus light irradiation). (a) Scheme displaying the design and analyses of the animal experiments. (b) Representative time-dependent photographs of the *S. aureus*-infected wounds of mice taken after different treatments. (c) Overlapped simulated wound areas within 11 days corresponding to (b). (d) Time-dependent relative wound sizes of the mice after different treatments. Data are presented as mean value ± SD ($n = 3$). (e) Representative photographs (taken on day 11) of the *S. aureus* bacterial colonies formed from the homogenized infected wound tissue dispersions of the mice that were subjected to different treatments. (f) Colony numbers (determined on day 11) of *S. aureus* cells in the wound areas of the mice after different treatments. (g) Giemsa staining results of the wound tissues from the mice on day 3 and 7 after different treatments (red arrows: bacteria). One-way ANOVA with Tukey's post-hoc test was used for the significance analysis between multiple groups. **$P < 0.01$, and ****$P < 0.0001$ for the OBC-P and OBC-PR groups versus the OBC group.

10.5)%). On the 11th day, the wounds in the OBC-PR + light group were almost healed, achieving a relative wound size of (12.6 ± 1.0)%, and the wounds were covered by new epithelial tissues. By contrast, on the 11th day, the relative wound sizes in the OBC + light and OBC-P + light groups were (42.1 ± 0.7)%, and (25.3 ± 3.5)%, respectively. All the above results demonstrated the excellent wound healing effect of the OBC-PR film (plus light irradiation). On the other hand, the bacterial counts of the infected wound sites were determined via the agar plate-based bacterial colony counting of the homogenized wound tissue samples. As shown in Fig. 6e and f, the numbers of bacterial colonies in the OBC-PR + light group reduced significantly to 4.9×10^4 CFU/g, while those in the OBC + light and OBC-P + light groups were 2.3×10^7 and 8.8×10^6 CFU/g, respectively.

Moreover, Giemsa staining of the wound tissues was also performed to evaluate the tissue regeneration states of the wounds after treatment with OBC, OBC-P, or OBC-PR as well as light irradiation on day 3 and 7 (Fig. 6g). On day 3, the OBC + light group showed a large number of bacteria in the wound area as shown in Fig. 6g (the red arrows). The OBC-P + light group also had bacteria, but the number was much smaller than that of the OBC + light group, indicating that the infection was not as serious as that in the OBC + light group. By contrast, in the OBC-PR + light group, almost no bacteria were found. On day 7, there were still a certain number of bacteria in the OBC + light and OBC-P + light groups, and there were almost no bacterial cells found in OBC-PR + light group, indicating that the OBC-PR film showed excellent in vivo antibacterial activity under light irradiation. In summary, the above

results all confirmed the excellent wound healing promotion and in vivo antibacterial performance of the OBC-PR film with light irradiation. Without light irradiation, the relative wound sizes in the OBC, OBC-P, and OBC-PR groups reduced to (30.4 ± 6.8)%, (17.3 ± 1.0)%, and (18.7 ± 0.2)%, respectively, on the 11th day (Fig. S11a−c). On the other hand, the numbers of bacterial colonies in the OBC-P and OBC-PR groups were reduced to 4.2×10^6 and 3.3×10^6, respectively (Fig. S11d), which were still higher than that of the OBC-PR + light group (Fig. 6f). The Giemsa staining results also supported the above data (Fig. S11e). All these results indicated that the OBC-P and OBC-PR films exhibited a remarkable antibacterial effect with no obvious difference without light irradiation, and the wound healing promotion effect of the three types of films also showed no significant difference without light irradiation. For OBC-PR, when light irradiation was applied, its antibacterial effect and wound healing promotion capacity were enhanced with the help of PDT.

2.7. Histological and immunofluorescence analyses

There are four main stages for wound healing, including hemostasis, inflammation process, cell proliferation, and skin tissue remodeling [69, 70]. The inflammation stage is one of the important steps during the complex wound healing process [71]. After the inflammation stage, the skin wounds will undergo the proliferation and remodeling stages [72]. To evaluate the neurogenesis and angiogenesis of the wound tissue after different treatments, we performed H&E and immunofluorescence

staining of the wound tissues with CD31 (red fluorescence) and β3-tubulin (green fluorescence). As shown in Fig. S12a, a large number of neutrophile granulocytes were observed in the tissue of the OBC + light group on day 3, while the number of neutrophile granulocytes in the OBC-P + light and OBC-PR + light groups decreased significantly. Especially, in the OBC-PR + light group, the number of neutrophile granulocytes was the least, indicating that the mice in the OBC-P + light and OBC-PR + light groups had passed through the acute inflammation phase, while the OBC + light group was still in the acute inflammation period. Besides, the hair follicles (green arrows) were observed in the

OBC-PR + light group, indicating that OBC-PR plus light could effectively promote hair follicle neogenesis. Compared with the OBC + light group, more blood vessels (black arrows) were also found in the OBC-P + light and OBC-PR + light groups. Without light irradiation, the OBC-P and OBC-PR films also exhibited antiinflammatory effect and collagen deposition (Fig. S11f), suggesting that OBC-P is also an effective wound dressing material.

To further investigate the tissue structure and the wound healing process, the wound tissues of the mice after different treatments were taken and analyzed by H&E staining, Masson's trichrome staining, Sirius
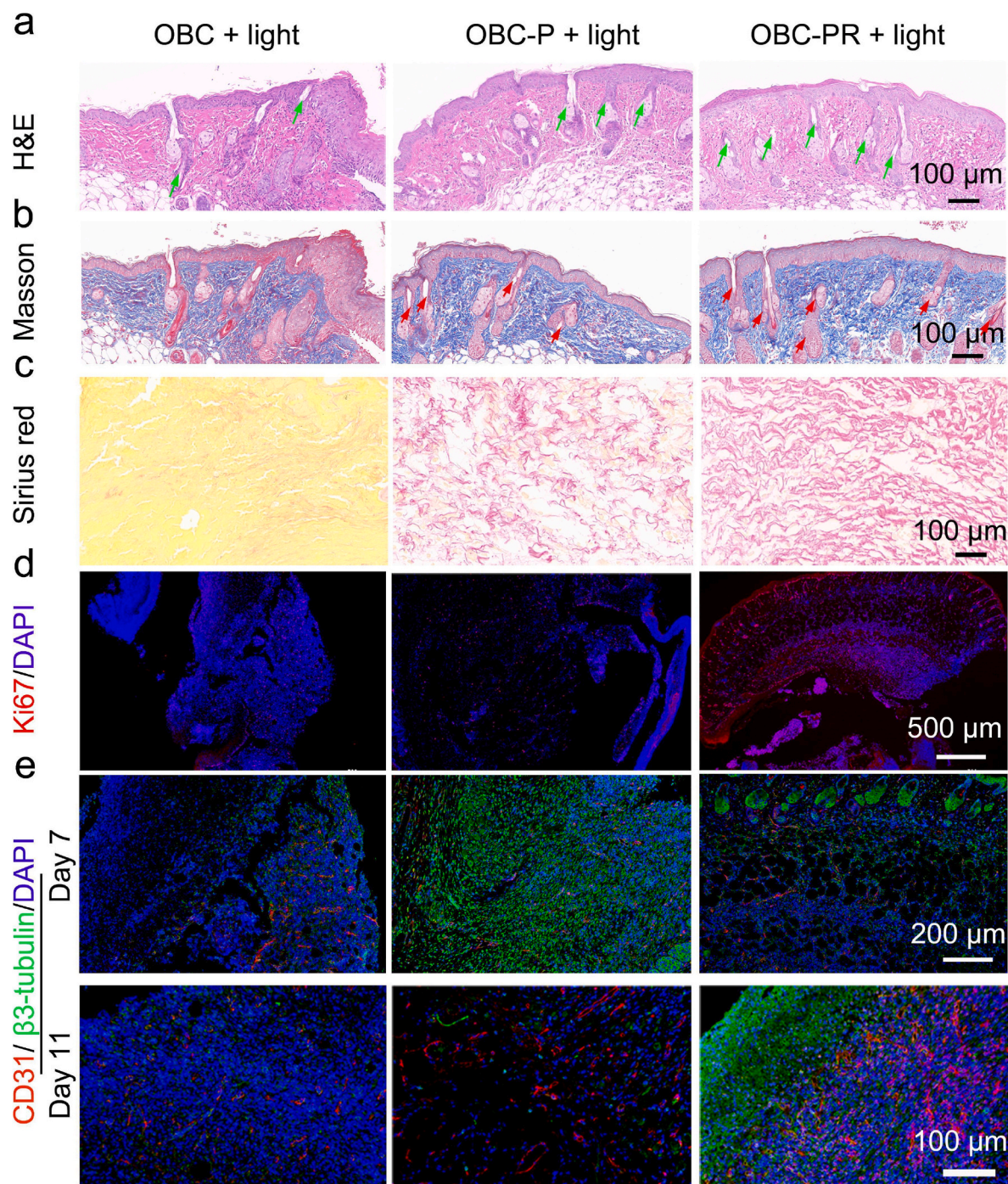

Fig. 7. Histological evaluations of the wounds treated with OBC, OBC-P, or OBC-PR films with light irradiation. (a–c) H&E, Masson's trichrome, and Sirius red staining results of the wound tissues from the mice after different treatments. (d,e) Ki67/DAPI (DAPI: 4′,6-diamidino-2-phenylindole dihydrochloride) and CD31/β3-tubulin/DAPI immunofluorescence staining results of the wound tissues from the mice after different treatments. The images in (a–d) are the wound tissue slices from the mice on day 7 after different staining treatments, and the images in (e) are the wound tissue slices from the mice on day 7 and day 11 after staining treatments.

red staining, and immunofluorescence analyses. As shown in the H&E results (Fig. 7a and S12a), the number of the inflammatory cells was significantly reduced on day 7 compared with that on day 3 for all groups. On day 7, the OBC-PR + light group had fewer inflammatory cells compared with the other groups and displayed more hair follicles (green arrows) (Fig. 7a), indicating the strong potential of the OBC-PR film in skin repair under light irradiation. Moreover, compared with the OBC + light group, the OBC-P + light and OBC-PR + light groups both promoted fibroblast migration as shown in the Masson's trichrome staining results (Fig. 7b). Moreover, skin appendages such as hair follicles were observed in the reconstituted dermal tissue of the OBC-P + light and OBC-PR + light groups (Fig. 7a and b), revealing that the wounds of the mice were well repaired.

In addition, since the collagen deposition is one of the important indicators for characterizing the skin tissue regeneration in wound healing process, we also evaluated the collagen formation by Masson's trichrome staining and Sirius red staining (Fig. S12b, Fig. 7b and c). Collagen fibers are marked as blue in the Masson's trichrome staining results of the wound tissue sections. On day 7, the OBC-PR + light group showed more collagen fiber deposition than the OBC + light group as reflected by the deeper blue color. Collagen deposition in the OBC-P + light group was also higher than that of the OBC + light group. The higher collagen deposition can accelerate the wound healing process and promote the skin tissue regeneration. Sirius red staining further revealed the composition and arrangement of collagen in the wound tissues. As shown in Fig. 7c, obvious collagen deposition was observed in the OBC-P + light and OBC-PR + light groups, indicating they had a strong ability in promoting wound healing. Without light irradiation, H&E, Masson's trichrome, and Sirius red staining all showed that the OBC-P and OBC-PR groups also showed more obvious neoepithelial tissue formation and collagen deposition (Fig. S13), indicating that the OBC-P and OBC-PR films also had a more obvious effect on promoting wound healing without light irradiation compared with the OBC + light group after 7 days of treatment. All these results indicated that the OBC-PR film can effectively promote wound healing by accelerating wound tissue reconstruction and healing rate. We also investigated the hair follicle proliferation via Ki67 staining. As shown in Fig. 7d, compared with the OBC + light and OBC-P + light groups, the Ki67 staining of the tissue in the OBC-PR + light group after 7 days of treatment had the strongest fluorescence signals, indicating that the most hair follicles were formed in this group. Moreover, in the wound healing process, dysregulated and insufficient revascularization will result in the impaired wound healing and regeneration due to the cell death and growth of necrotic tissue areas [73]. Some strategies have been applied to promote the revascularization of the microenvironment in the wound tissue [73,74]. For example, Später et al. fabricated a functional biomaterial, the microparticles of solidified secretome (MIPSOS), which can accumulate various pro-angiogenic factors, thereby accelerating revascularization and wound healing [73]. On day 7, the fluorescence of CD31 and β3-tubulin was hardly observed in the OBC + light group (Fig. 7e); in contrast, much more fluorescence was observed in the OBC-P + light and OBC-PR + light groups, indicating that the blood vessels and nerves were regenerated gradually in these two groups. On day 11, the expression of CD31 and β3-tubulin was hardly observed in the OBC + light group. However, the OBC-PR + light group showed obvious fluorescence signals of CD31 and β3-tubulin, indicating that there was a certain degree of angiogenesis and vascularization in the wound tissues after treatment with the OBC-PR film and light irradiation, revealing that OBC-PR could promote wound healing under light irradiation.

2.8. Macrophage polarization and angiogenesis

Macrophages as the innate immune cells play an important role in modulating the immune responses in the wound healing process [71]. Macrophage polarization that involves the transition of the classically activated macrophages (M1) and alternatively activated macrophages (M2) is the way that macrophages regulate the immune system to promote wound healing [75]. The M1 macrophages appear in the early proinflammatory stage that leads to serious inflammation reaction, while M2 macrophages regulate the transition from the inflammatory stage to the proliferative stage [75]. To evaluate the macrophage polarization in the wound environment after different treatments in the wound healing process, we performed the immunofluorescence staining of the wound tissues with inducible nitric oxide synthase (iNOS) (M1 marker) and CD206 (M2 marker) on day 3 and day 7. As shown in Fig. S14a, on day 3, the macrophages of the wound tissue after OBC + light or OBC-P + light treatment were in the M1 phase; however, the OBC-PR + light group entered the M1/M2 equilibrium stage. As shown in Fig. 8a and e, after 7 days of treatment, the fluorescence signals of iNOS in the OBC-P + light and OBC-PR + light groups were both greatly decreased compared with those in the OBC + light group and the fluorescence intensities of CD206 in the OBC-P + light and OBC-PR + light groups were much higher than that of the OBC + light group, indicating that the OBC-P and OBC-PR films significantly decreased the percentage of M1 cells and increased the percentage of M2 cells in the wound tissue after light irradiation. The quantitative statistical analysis of the tissues treated with different films also revealed that the relative expression of CD206 in the OBC-P + light and OBC-PR + light groups was increased and the relative expression of iNOS in OBC-P + light and OBC-PR + light groups was reduced. The results demonstrated that the OBC-P and OBC-PR films plus light irradiation could effectively promote the M1-to-M2 macrophage polarization, which facilitated the transition from inflammation phase to proliferation phase of the wound healing process. In addition, the wound healing process involves the changes of many types of cytokines, such as the proinflammatory factors, including tumor necrosis factor-α (TNF-α), interleukin-6 (IL-6), and vascular endothelial growth factor (VEGF). To further evaluate the way in which the photosensitizable OBC-PR film promoted skin wound healing, the immunofluorescence staining of IL-6, TNF-α, and VEGF was performed to evaluate the inflammatory reaction and the angiogenesis behavior during the wound healing process. As shown in Fig. S14b and S14c, on day 3, the wounds with OBC + light or OBC-P + light treatment showed a serious inflammatory reaction. However, the OBC-PR + light group exhibited a weaker inflammatory reaction. After 7 days of treatment, the expression of TNF-α and IL-6 in the OBC-P + light and OBC-PR + light groups was lower than that in the OBC + light group. Especially, in the OBC-PR + light group, the expression of TNF-α and IL-6 was significantly inhibited (Fig. 8b and c). The quantitative results shown in Fig. 8f also supported the above conclusion. In addition, as shown in Fig. S14d, the expression of VEGF in all groups on day 3 was low; however, the immunofluorescence of VEGF in the OBC-P + light and OBC-PR + light groups was significantly enhanced compared with that in the OBC group after 7 days, further confirming the angiogenesis promotion effect of the OBC-P and OBC-PR films under light irradiation (Fig. 8d). The quantitative result was also consistent with the above conclusion (Fig. 8g). All the above data showed that the OBC-P and OBC-PR films can effectively promote the infected wound healing by regulating the macrophage polarization, reducing the proinflammatory factors, and facilitating the angiogenesis under light irradiation condition.

2.9. Biodegradability and biocompatibility of the OBC, OBC-P, and OBC-PR films

Considering the environmental friendliness and the safety of the wound dressings, the optimal wound dressings should be biodegradable and biocompatible. Therefore, we detected the biodegradability and biocompatibility characteristics of the films. The in vitro biodegradability of the films was detected according to the methods reported by Mao et al. [76]. The results in Fig. 9a showed that both OBC-P and OBC-PR films were gradually degraded as time went by under the action of the crude cellulase complex. However, the OBC film was only
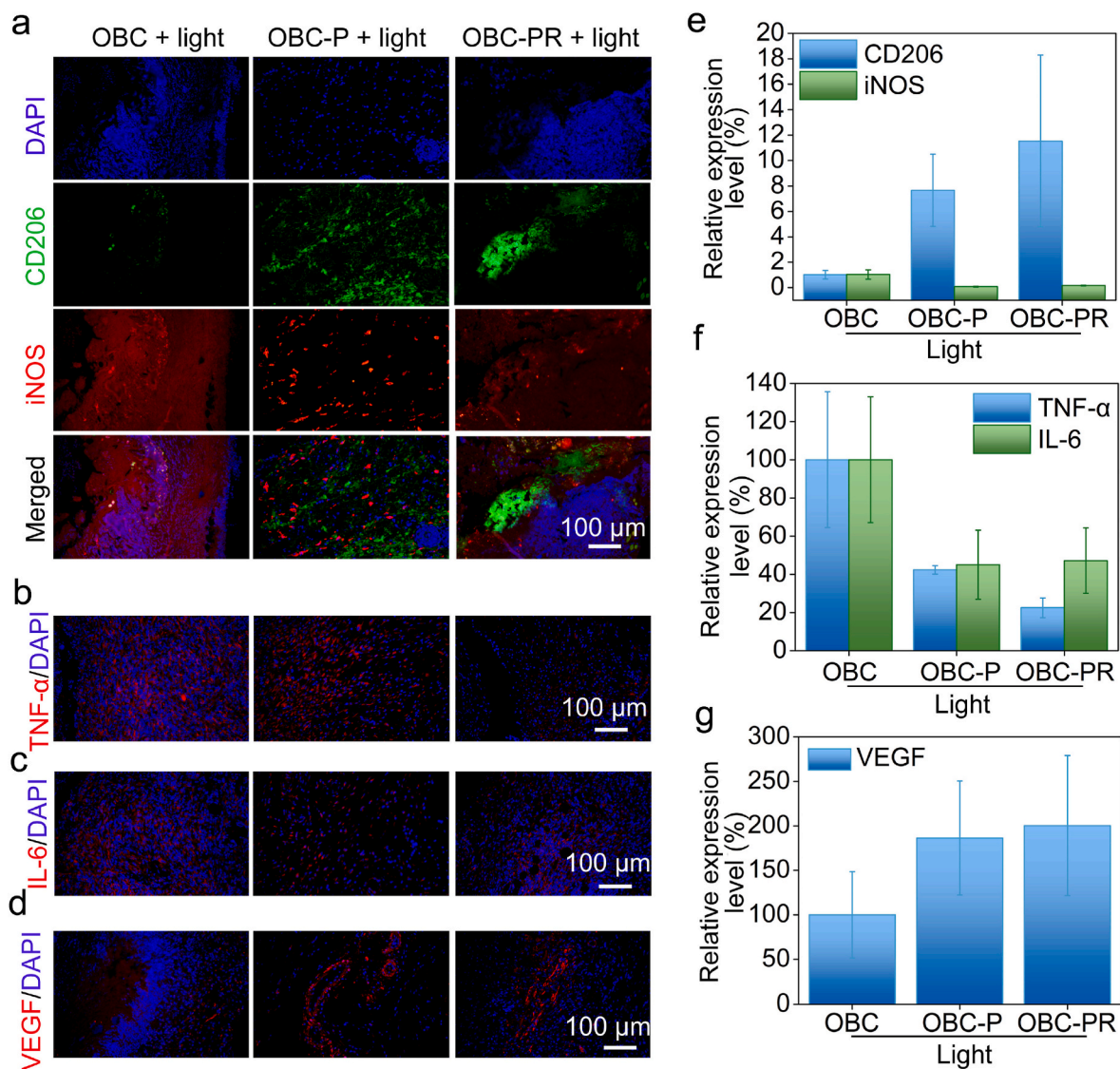
Fig. 8. Macrophage polarization, antiinflammatory activities, and angiogenesis effects of the OBC, OBC-P, and OBC-PR films under light irradiation. (a) Immunofluorescence images (taken on day 7) of the wound tissues after various treatments. Before imaging, the tissues were stained with DAPI, CD206, and iNOS. (b–d) Immunofluorescence images (taken on day 7) of TNF-α, IL-6, and VEGF expressed in the wound tissues. (e–g) Relative expression levels of CD206, iNOS, TNF-α, IL-6, and VEGF in the wound tissues.

partially degraded. As shown in Fig. 9b, at 300 min, the content of total sugar in the degradation solution of the OBC-PR film was 0.58 mg/mL, which was higher than that in the OBC degradation solution (0.41 mg/mL). The total sugar in the degradation solution of the OBC-P film was very similar to that of the OBC-PR film, suggesting the OBC-P and OBC-PR films were biodegradable and degraded faster than the pure OBC film under the action of cellulase. Such a degradation property of OBC-P and OBC-PR films demonstrated their environmental friendliness, avoiding the environmental pollution. More importantly, the degraded products can be reused as medium components to produce BC hydrogel (Fig. 9c), which realized the recycling utilization of the wound dressing materials, showing a high economic property.

It has been reported that BC-based materials show excellent biocompatibility [77]. In our present work, the hemolysis rate and in vivo safety evaluation of the OBC, OBC-P, and OBC-PR films were evaluated according to the previously reported methods [78–80]. As shown in Fig. S15, there was no obvious difference between the phosphate-buffered saline (PBS) (the negative control) and film groups, showing that no noticeable hemolysis was induced by the OBC, OBC-P, and OBC-PR films. In addition, the in vivo biosafety evaluation was also

carried out. As shown in Fig. 9d, all the films showed excellent in vivo safety, which makes them practically applicable in the in vivo biomedical applications.

3. Conclusion

In this work, we constructed a multifunctional BC-based antibacterial wound dressing (the OBC-PR film) based on the reaction among OBC, PHGH, and RB for achieving a dual effect of PHGH-based chemotherapy and PDT for antibacterial treatment. Compared with the OBC film, the OBC-P and OBC-PR films exhibited excellent bacterial capture ability due to their rough surface structure. Furthermore, the OBC-PR films could rapidly and effectively inhibit the growth of both *E. coli* and *S. aureus* cells through the synergistic effect of PHGH and the ROS produced by RB under white light irradiation. More interestingly, the OBC-PR film could regulate the balance of M1/M2 macrophages, inhibiting the inflammatory reaction. Subsequently, the OBC-PR film effectively promoted the blood vessel and nerve regeneration, significantly promoting wound healing. In addition, as a wound dressing material, OBC-PR was safe, biodegradable, and regeneratable,
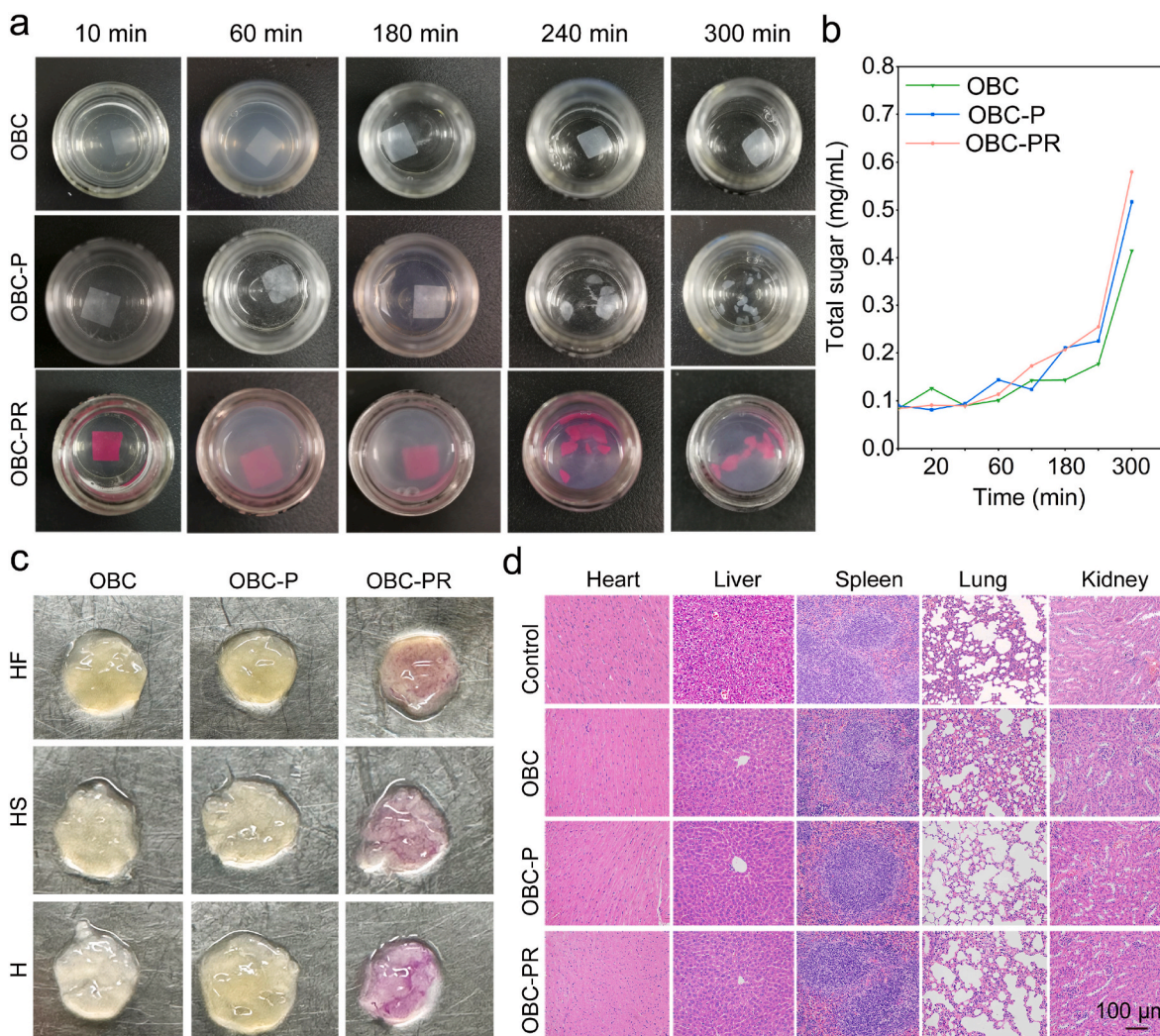
Fig. 9. Biodegradability and in vivo biosafety evaluations of the OBC, OBC-P, and OBC-PR films. (a) Photographs showing the cellulase-treated OBC, OBC-P, and OBC-PR films (dispersed in 50 mM HAc/NaAc buffer, pH 4.8) for different time periods. (b) Total sugar contents in the cellulase-treated OBC, OBC-P, and OBC-PR films (dispersed in 50 mM HAc/NaAc buffer, pH 4.8) measured at different time points. (c) Reproduced BC by using the degraded OBC-based films (as shown in a) as the medium components. H: the enzymatic hydrolyzates of the films; HF: the H supplemented with complete fermented medium without carbon sources; HS: the supplemented H with 5 g/L yeast extract and tryptone. (d) *S*afety evaluation results of OBC, OBC-P, and OBC-PR films in a mouse model by H&E staining analysis of the hearts, livers, spleens, lungs, and kidneys collected from the mice on day 30 after treatment with different films.

indicating its enormous potential for wound healing application and clinical translation as a sustainable and green material. Collectively, the present work provides a multifunctional platform capable of promoting the infected wound healing via the synergistic vasculature/nerve/immunocyte remodeling promoted by a cooperative PDT and chemo-therapy effect, which may have implications for the future development of multifunctional wound dressing materials. The simplicity of the fabrication process and the excellent wound healing-promoting ability of the OBC-PR films are attractive features that can lead to more prac-tical applications in combating microbes and their biofilms, and pro-moting the infected wound healing. In addition, based on the antiviral ability of the guanidine-based polymers, the potential use of the OBC-PR film as an antiviral material should be explored in the future. It is also expected that the OBC-PR films can be incorporated into textiles for more versatile antimicrobial and antiviral uses.

4. Experimental section

4.1. Materials

BC was obtained from the culture of *A. xylinum* according to the

previously reported method [81]. Briefly, *A. xylinum* was first cultured in a seed culture medium at 30 °C and 150 rpm for 2 days, and then 7 vol % of the obtained bacterial culture was transferred into the fermentation medium (30 mL, in a culture dish with a diameter of 9 cm) and cultured at 30 °C for another 5–7 days until the culture medium was completely utilized by *A. xylinum*. The obtained BC was immersed in deionized water several times until the membrane became white and translucent, and then treated with 0.3 wt% sodium hydroxide (NaOH) solution and 0.09 vol% hydrogen peroxide solution at 80 °C for 30 min to inactivate the bacteria and proteins, and subsequently washed with deionized water thoroughly until the pH reached 7.0. PHGH (average molecular weight: ~2600 Da) was synthesized in our lab. RB, EDC•HCl, and NHS were purchased from Sigma-Aldrich (Shanghai, China). Dialysis bags with the molecular weight cut-off (MWCO) of 14 kDa were from Spec-trum Labs (Rancho Dominguez, CA, USA). Other chemicals used in this study were of analytical grade.

4.2. Preparation of OBC, OBC-P, and OBC-PR films

BC was first cut into pieces using a scissor and suspended in water, and the pH of the obtained suspension was adjusted with NaOH to above

10. Then TEMPO, NaBr, and NaClO were sequentially added into the above BC suspension to achieve the final concentrations of 0.2 mmol/g (dried BC), 10 mmol/g (dried BC), and 0.5 mol/g (dried BC) for TEMPO, NaBr, NaClO, respectively. After 1 h of reaction, 12.5 mL ethanol was added to stop the reaction, and the pH was adjusted to 6–7 with HCl. The obtained OBC was dialyzed, washed with water, and pulped with a juicer to obtain OBC suspension. Then, PHGH or PHGH and RB were conjugated onto OBC by the EDC/NHS method. Briefly, the pH of the above-obtained OBC dispersion (150 mL) was adjusted to < 6 using HCl solution (1 M). Then, for OBC-PR suspension, RB (15 mg) was added into the OBC suspension. Afterward, 1500 μL EDC•HCl (14 mg/mL) was added and stirred at 300 rpm for 10 min, and then 1500 μL NHS (13.4 mg/mL) was added and stirred at 90 rpm for 1 h. 117 mg PHGH was added to the above solution and stirred at 90 rpm for 24 h. Finally, the above suspension was dialyzed with a dialysis bag (MWCO of 14 kDa) against deionized water for 3 days to obtain the OBC-PR suspension. The preparation procedure of OBC-P suspension was similar to that of OBC-PR but without the addition of RB. Finally, the OBC, OBC-P, and OBC-PR films were formed by vacuum filtration and pressing treatment of the above OBC, OBC-P, and OBC-PR suspensions.

4.3. Other experimental details

Other experimental details including characterization, ROS generation assessment of the films, evaluation of the bacteria-capturing ability of the OBC, OBC-P, and OBC-PR films, antibacterial activity assessments, antibacterial mechanism investigations, biofilm inhibition assay, in vivo antibacterial activity and wound healing ability assays, biodegradation and biocompatibility evaluation, and statistical analysis can be found in the Supporting Information.

Ethics approval and consent to participate

The BALB/c mice (6 weeks old) were purchased from Jiangsu Huachuang Xinnuo Pharmaceutical Technology Co., Ltd (Taizhou, China), and all the animal experiments were performed according to the relevant protocols approved by the Animal Care Committee of Southeast University (approval number: 20230110005).

Data availability

Experimental data from this study are available from Chengcheng Li, Huining Xiao, or Fu-Gen Wu upon reasonable request.

CRediT authorship contribution statement

Chengcheng Li: Writing – review & editing, Writing – original draft, Validation, Supervision, Resources, Project administration, Methodology, Funding acquisition, Formal analysis, Data curation, Conceptualization. **Ya-Xuan Zhu:** Methodology, Investigation, Formal analysis. **Ying Yang:** Resources, Methodology, Investigation. **Wanting Miao:** Software, Resources, Investigation. **Xiaotong Shi:** Software, Investigation. **Ke-Fei Xu:** Resources, Investigation. **Zi-Heng Li:** Resources, Investigation. **Huining Xiao:** Writing – review & editing, Validation, Conceptualization. **Fu-Gen Wu:** Writing – review & editing, Validation, Resources, Conceptualization.

Declaration of competing interest

The authors declare that they have no known competing financial interests or personal relationships that could have appeared to influence the work reported in this paper.

Acknowledgements

Appendix A. Supplementary data

Supplementary data to this article can be found online at https://doi.org/10.1016/j.bioactmat.2024.06.031.

References

[1] T.A. Harris-Tryon, E.A. Grice, Microbiota and maintenance of skin barrier function, Science 376 (2022) 940–945.
[2] C. Cui, S. Sun, X. Li, S. Chen, S. Wu, F. Zhou, J. Ma, Optimizing the chitosan-PCL based membranes with random/aligned fiber structure for controlled ciprofloxacin delivery and wound healing, Int. J. Biol. Macromol. 205 (2022) 500–510.
[3] Y. Liang, J. He, B. Guo, Functional hydrogels as wound dressing to enhance wound healing, ACS Nano 15 (2021) 12687–12722.
[4] R. Dong, B. Guo, Smart wound dressings for wound healing, Nano Today 41 (2021) 101290.
[5] Q. Xin, H. Shah, A. Nawaz, W. Xie, M.Z. Akram, A. Batool, L. Tian, S.U. Jan, R. Boddula, B. Guo, Q. Liu, J.R. Gong, Antibacterial carbon-based nanomaterials, Adv. Mater. 31 (2019) 1804838.
[6] M.I. Hutchings, A.W. Truman, B. Wilkinson, Antibiotics: past, present and future, Curr. Opin. Microbiol. 51 (2019) 72–80.
[7] H. Bai, H. Yuan, C. Nie, B. Wang, F. Lv, L. Liu, S. Wang, A supramolecular antibiotic switch for antibacterial regulation, Angew. Chem. Int. Ed. 54 (2015) 13208–13213.
[8] Q. Cheng, M. Xu, C. Sun, K. Yang, Z. Yang, J. Li, J. Zheng, Y. Zheng, R. Wang, Enhanced antibacterial function of a supramolecular artificial receptor-modified macrophage (SAR-Macrophage), Mater. Horiz. 9 (2022) 934–941.
[9] T. Wang, D. Dong, T. Chen, J. Zhu, S. Wang, W. Wen, X. Zhang, H. Tang, J. Liang, S. Wang, H. Xiong, Acidity-responsive cascade nanoreactor based on metal-nanozyme and glucose oxidase combination for starving and photothermal-enhanced chemodynamic antibacterial therapy, Chem. Eng. J. 446 (2022) 137172.
[10] C. Jia, F.G. Wu, Antibacterial chemodynamic therapy: materials and strategies, BME Front. 4 (2023), 0021.
[11] C. Jia, Y. Guo, F.G. Wu, Chemodynamic therapy via Fenton and Fenton-like nanomaterials: strategies and recent advances, Small 18 (2022) 2103868.
[12] F. Lin, Q.Y. Duan, F.G. Wu, Conjugated polymer-based photothermal therapy for killing microorganisms, ACS Appl. Polym. Mater. 2 (2020) 4331–4344.
[13] Y. Chen, Y. Gao, Y. Chen, L. Liu, A. Mo, Q. Peng, Nanomaterials-based photothermal therapy and its potentials in antibacterial treatment, J. Contr. Release 328 (2020) 251–262.
[14] M. Liang, L. Shang, Y. Yu, Y. Jiang, Q. Bai, J. Ma, D. Yang, N. Sui, Z. Zhu, Ultrasound activatable microneedles for bilaterally augmented sono-chemodynamic and sonothermal antibacterial therapy, Acta Biomater. 158 (2023) 811–826.
[15] X. Zhou, Z. Wang, Y.K. Chan, Y. Yang, Z. Jiao, L. Li, J. Li, K. Liang, Y. Deng, Infection micromilieu-activated nanocatalytic membrane for orchestrating rapid sterilization and stalled chronic wound regeneration, Adv. Funct. Mater. 32 (2022) 2109469.
[16] C. Li, F. Lin, W. Sun, F.G. Wu, H. Yang, R. Lv, Y.X. Zhu, H.R. Jia, C. Wang, G. Gao, Z. Chen, Self-assembled rose bengal-exopolysaccharide nanoparticles for improved photodynamic inactivation of bacteria by enhancing singlet oxygen generation directly in the solution, ACS Appl. Mater. Interfaces 10 (2018) 16715–16722.
[17] J. Li, W. Sun, Z. Yang, G. Gao, H.H. Ran, K.F. Xu, Q.Y. Duan, X. Liu, F.G. Wu, Rational design of self-assembled cationic porphyrin-based nanoparticles for efficient photodynamic inactivation of bacteria, ACS Appl. Mater. Interfaces 12 (2020) 54378–54386.
[18] H.R. Jia, Y.X. Zhu, Z. Chen, F.G. Wu, Cholesterol-assisted bacterial cell surface engineering for photodynamic inactivation of Gram-positive and Gram-negative bacteria, ACS Appl. Mater. Interfaces 9 (2017) 15943–15951.
[19] X. Lin, Y. Fang, Z. Hao, H. Wu, M. Zhao, S. Wang, Y. Liu, Bacteria-triggered multifunctional hydrogel for localized chemodynamic and low-temperature photothermal sterilization, Small 17 (2021) 2103303.
[20] X. Bi, Q. Bai, M. Liang, D. Yang, S. Li, L. Wang, J. Liu, W.W. Yu, N. Sui, Z. Zhu, Silver peroxide nanoparticles for combined antibacterial sonodynamic and photothermal therapy, Small 18 (2022) 2104160.
[21] X. Sun, J. Sun, Y. Sun, C. Li, J. Fang, T. Zhang, Y. Wan, L. Xu, Y. Zhou, L. Wang, B. Dong, Oxygen self-sufficient nanoplatform for enhanced and selective antibacterial photodynamic therapy against anaerobe-induced periodontal disease, Adv. Funct. Mater. 31 (2021) 2101040.
[22] J. von Byern, I. Grunwald, Biological adhesive systems: from nature to technical and medical application, SpringerWien, NewYork (2010).
[23] X. Sun, P. Jia, H. Zhang, M. Dong, J. Wang, L. Li, T. Bu, X. Wang, L. Wang, Q. Lu, J. Wang, Green regenerative hydrogel wound dressing functionalized by natural drug-food homologous small molecule self-assembled nanospheres, Adv. Funct. Mater. 32 (2022) 2106572.
[24] Q. Zeng, X. Qi, G. Shi, M. Zhang, H. Haick, Wound dressing: from nanomaterials to diagnostic dressings and healing evaluations, ACS Nano 16 (2022) 1708–1733.

[25] S. Li, A. Chen, Y. Chen, Y. Yang, Q. Zhang, S. Luo, M. Ye, Y. Zhou, Y. An, W. Huang, T. Xuan, Y. Pan, X. Xuan, H. He, J. Wu, Lotus leaf inspired antiadhesive and antibacterial gauze for enhanced infected dermal wound regeneration, Chem. Eng. J. 402 (2020) 126202.

[26] K. Zhang, X. Bai, Z. Yuan, X. Cao, X. Jiao, Y. Li, Y. Qin, Y. Wen, X. Zhang, Layered nanofiber sponge with an improved capacity for promoting blood coagulation and wound healing, Biomaterials 204 (2019) 70–79.

[27] C. Gao, C.H.T. Kwong, M. Tang, J. Liu, H. Kam, S. Li, S.M.Y. Lee, C. Fan, H.Z. Yu, R. Wang, A bacterially engineered macrophage sponge as a neutralization decoy to treat bacterial infection, Matter 6 (2023) 3889–3911.

[28] M. He, F. Ou, Y. Wu, X. Sun, X. Chen, H. Li, D. Sun, L. Zhang, Smart multi-layer PVA foam/CMC mesh dressing with integrated multi-functions for wound management and infection monitoring, Mater. Des. 194 (2020) 108913.

[29] B.H. Shan, F.G. Wu, Hydrogel-based growth factor delivery platforms: strategies and recent advances, Adv. Mater. 36 (2024) 2210707.

[30] X. Zhang, Y. Li, D. He, Z. Ma, K. Liu, K. Xue, H. Li, An effective strategy for preparing macroporous and self-healing bioactive hydrogels for cell delivery and wound healing, Chem. Eng. J. 425 (2021) 130677.

[31] F. Wahid, L.H. Huang, X.Q. Zhao, W.C. Li, Y.Y. Wang, S.R. Jia, C. Zhong, Bacterial cellulose and its potential for biomedical applications, Biotechnol. Adv. 53 (2021) 107856.

[32] C. Zhou, Z. Yang, X. Xun, L. Ma, Z. Chen, X. Hu, X. Wu, Y. Wan, H. Ao, De novo strategy with engineering a multifunctional bacterial cellulose-based dressing for rapid healing of infected wounds, Bioact. Mater. 13 (2022) 212–222.

[33] J. Ahmed, M. Gultekinoglu, M. Edirisinghe, Bacterial cellulose micro-nano fibres for wound healing applications, Biotechnol. Adv. 41 (2020) 107549.

[34] B. Mbituyimana, L. Liu, W. Ye, B.O. Ode Boni, K. Zhang, J. Chen, S. Thomas, R. V. Vasilievich, Z. Shi, G. Yang, Bacterial cellulose-based composites for biomedical and cosmetic applications: research progress and existing products, Carbohydr. Polym. 273 (2021) 118565.

[35] D.Z. Zmejkoski, Z.M. Markovic, D.D. Mitic, N.M. Zdravkovic, N.O. Kozyrovska, N. Bugárová, B.M. Todorovic Markovic, Antibacterial composite hydrogels of graphene quantum dots and bacterial cellulose accelerate wound healing, J. Biomed. Mater. Res. 110 (2022) 1796–1805.

[36] E. Gutierrez, P.A. Burdiles, F. Quero, P. Palma, F. Olate-Moya, H. Palza, 3D printing of antimicrobial alginate/bacterial-cellulose composite hydrogels by incorporating copper nanostructures, ACS Biomater. Sci. Eng. 5 (2019) 6290–6299.

[37] L. Zhang, Y. Yu, S. Zheng, L. Zhong, J. Xue, Preparation and properties of conductive bacterial cellulose-based graphene oxide-silver nanoparticles antibacterial dressing, Carbohydr. Polym. 257 (2021) 117671.

[38] X. Liu, M. Wu, M. Wang, Q. Hu, J. Liu, Y. Duan, B. Liu, Direct synthesis of photosensitizable bacterial cellulose as engineered living material for skin wound repair, Adv. Mater. 34 (2022) 2109010.

[39] Y. He, J. Leng, K. Li, K. Xu, C. Lin, Z. Yuan, R. Zhang, D. Wang, B. Tao, T.J. Huang, A multifunctional hydrogel coating to direct fibroblast activation and infected wound healing via simultaneously controllable photobiomodulation and photodynamic therapies, Biomaterials 278 (2021) 121164.

[40] D.Z. Zmejkoski, N.M. Zdravkovic, M. Budimir Filimonović, V.B. Pavlović, S. V. Butulija, D.D. Milivojević, Z.M. Marković, B.M. Todorović Marković, Reduction in pathogenic biofilms by the photoactive composite of bacterial cellulose and nanochitosan dots under blue and green light, J. Funct. Biomater. 15 (2024) 72.

[41] Z.M. Marković, D.Z. Zmejkoski, M.D. Budimir, N. Bugarova, A. Kleinova, S. B. Kuzman, Z. Špitalský, V.B. Pavlović, D.D. Milivojević, B.M. Todorović Marković, Photoactive graphene quantum dots/bacterial cellulose hydrogels: structural, mechanical, and pro-oxidant study, J. Appl. Polym. Sci. 139 (2022) 51996.

[42] Y. Feng, C.C. Tonon, S. Ashraf, T. Hasan, Photodynamic and antibiotic therapy in combination against bacterial infections: efficacy, determinants, mechanisms, and future perspectives, Adv. Drug Deliv. Rev. 177 (2021) 113941.

[43] Z. Li, S. Lu, W. Liu, T. Dai, J. Ke, X. Li, R. Li, Y. Zhang, Z. Chen, X. Chen, Synergistic lysozyme-photodynamic therapy against resistant bacteria based on an intelligent upconversion nanoplatform, Angew. Chem. Int. Ed. 60 (2021) 19201–19206.

[44] Z. Zhu, L. Wang, Y. Peng, X. Chu, L. Zhou, Y. Jin, H. Guo, Q. Gao, J. Yang, X. Wang, Continuous self-oxygenated double-layered hydrogel under natural light for real-time infection monitoring, enhanced photodynamic therapy, and hypoxia relief in refractory diabetic wounds healing, Adv. Funct. Mater. 32 (2022) 2201875.

[45] J. Gao, L. Hao, R. Jiang, Z. Liu, L. Tian, J. Zhao, W. Ming, L. Ren, Surprisingly fast assembly of the MOF film for synergetic antibacterial phototherapeutics, Green Chem. 24 (2022) 5930–5940.

[46] D. Wang, H. Wu, G. Yang, C. Qian, L. Gu, H. Wang, W. Zhou, J. Liu, Y. Wu, X. Zhang, Metal–organic framework derived multicomponent nanoagent as a reactive oxygen species amplifier for enhanced photodynamic therapy, ACS Nano 14 (2020) 13500–13511.

[47] Y. Sang, W. Li, L. Liu, L. Zhang, H. Wang, Z. Liu, J. Ren, X. Qu, Construction of nanozyme-hydrogel for enhanced capture and elimination of bacteria, Adv. Funct. Mater. 29 (2019) 1900518.

[48] Z. Zhang, H. Yan, B. Qiu, P. Ran, W. Cao, X. Jia, K. Huang, X. Li, Persistent luminescence-based theranostics for real-time monitoring and simultaneously launching photodynamic therapy of bacterial infections, Small 18 (2022) 2200813.

[49] H. Hu, D. Zhong, W. Li, X. Lin, J. He, Y. Sun, Y. Wu, M. Shi, X. Chen, F. Xu, Microalgae-based bioactive hydrogel loaded with quorum sensing inhibitor promotes infected wound healing, Nano Today 42 (2022) 101368.

[50] T. Bottcher, I. Kolodkin-Gal, R. Kolter, R. Losick, J. Clardy, Synthesis and activity of biomimetic biofilm disruptors, J. Am. Chem. Soc. 135 (2013) 2927–2930.

[51] A. Antonoplis, X.Y. Zang, M.A. Huttner, K.K.L. Chong, Y.B. Lee, J.Y. Co, M. R. Amieva, K.A. Kline, P.A. Wender, L. Cegelski, A dual-function antibiotic-

[52] transporter conjugate exhibits superior activity in sterilizing MRSA biofilms and killing persister cells, J. Am. Chem. Soc. 140 (2018) 16140–16151.

[52] M.K. Oule, R. Azinwi, A.M. Bernier, T. Kablan, A.M. Maupertuis, S. Mauler, R. K. Nevry, K. Dembele, L. Forbes, L. Diop, Polyhexamethylene guanidine hydrochloride-based disinfectant: a novel tool to fight meticillin-resistant *Staphylococcus aureus* and nosocomial infections, J. Med. Microbiol. 57 (2008) 1523–1528.

[53] S. Demartis, A. Obinu, E. Gavini, G. Giunchedi, G. Rassu, Nanotechnology-based rose bengal: a broad-spectrum biomedical tool, Dyes Pigments 188 (2021) 109236.

[54] S. Zamani Taghizadeh Rabe, S.H. Mousavi, N. Tabasi, M. Rastin, S. Zamani Taghizadeh Rabe, Z. Siadat, M. Mahmoudi, Rose bengal suppresses gastric cancer cell proliferation via apoptosis and inhibits nitric oxide formation in macrophages, J. Immunot. 11 (2014) 367–375.

[55] N. Mori, H. Kawasaki, E. Nishida, Y. Kanemoto, H. Miyaji, J. Umeda, Rose bengal-decorated rice husk-derived silica nanoparticles enhanced singlet oxygen generation for antimicrobial photodynamic inactivation, J. Mater. Sci. 58 (2023) 2801–2813.

[56] D. Gan, T. Xu, W. Xing, X. Ge, L. Fang, K. Wang, F. Ren, X. Lu, Mussel-inspired contact-active antibacterial hydrogel with high cell affinity, toughness, and recoverability, Adv. Funct. Mater. 29 (2019) 1805964.

[57] J. Li, Y. Wang, J. Yang, W. Liu, Bacteria activated-macrophage membrane-coated tough nanocomposite hydrogel with targeted photothermal antibacterial ability for infected wound healing, Chem. Eng. J. 420 (2021) 127638.

[58] G.M. Lanno, C. Ramos, L. Preem, M. Putrins, I. Laidmae, T. Tenson, Antibacterial porous electrospun fibers as skin scaffolds for wound healing applications, ACS Omega 5 (2020) 30011–30022.

[59] J. Chi, C. Shao, L. Shang, Y. Zhao, F. Ye, Microfluidic droplet templates derived porous patch with anisotropic wettability, Chem. Eng. J. 417 (2021) 128073.

[60] Y. Arima, H. Iwata, Effect of wettability and surface functional groups on protein adsorption and cell adhesion using well-defined mixed self-assembled monolayers, Biomaterials 28 (2007) 3074–3082.

[61] X. Qi, Y. Huang, S. You, Y. Xiang, E. Cai, R. Mao, W. Pan, X. Tong, W. Dong, F. Ye, J. Shen, Engineering robust Ag-decorated polydopamine nano-photothermal platforms to combat bacterial infection and prompt wound healing, Adv. Sci. 9 (2022) 2106015.

[62] Y. Hu, J.M. Catchmark, In vitro biodegradability and mechanical properties of bioabsorbable bacterial cellulose incorporating cellulases, Acta Biomater. 7 (2011) 2835–2845.

[63] W. Li, E.S. Thian, M. Wang, Z. Wang, L. Ren, Surface design for antibacterial materials: from fundamentals to advanced strategies, Adv. Sci. 8 (2021) 2100368.

[64] J. He, Z. Zheng, M.C.L. Irene, Different responses of Gram-negative and Gram-positive bacteria to photocatalytic disinfection using solar-light-driven magnetic TiO$_2$-based material, and disinfection of real sewage, Water Res. 207 (2021) 117816.

[65] T.A. Dahl, W.R. Midden, P.E. Hartman, Comparison of killing of Gram-negative and Gram-positive bacteria by pure singlet oxygen, J. Bacteriol. 171 (1989) 2188–2194.

[66] J. Zhang, P. Su, H. Chen, M. Qiao, B. Yang, X. Zhao, Impact of reactive oxygen species on cell activity and structural integrity of Gram-positive and Gram-negative bacteria in electrochemical disinfection system, Chem. Eng. J. 451 (2023) 138879.

[67] K.B. Steinbuch, M. Fridman, Mechanisms of resistance to membrane-disrupting antibiotics in Gram-positive and Gram-negative bacteria, MedChemComm 7 (2016) 86–102.

[68] E.R. Rojas, G. Billings, P.D. Odermatt, G.K. Auer, L. Zhu, A. Miguel, F. Chang, D. B. Weibel, J.A. Theriot, K.C. Huang, The outer membrane is an essential load-bearing element in Gram-negative bacteria, Nature 559 (2018) 617–621.

[69] R. Li, K. Liu, X. Huang, D. Li, J. Ding, B. Liu, X. Chen, Bioactive materials promote wound healing through modulation of cell behaviors, Adv. Sci. 9 (2022) 2105152.

[70] A. Nourian Dehkordi, F. Mirahmadi Babaheydari, M. Chehelgerdi, S. Raeisi Dehkordi, Skin tissue engineering: wound healing based on stem-cell-based therapeutic strategies, Stem Cell Res. Ther. 10 (2019) 111.

[71] N. Xu, Y. Gao, Z. Li, Y. Chen, M. Liu, J. Jia, R. Zeng, G. Luo, J. Li, Y. Yu, Immunoregulatory hydrogel decorated with tannic acid/ferric ion accelerates diabetic wound healing via regulating macrophage polarization, Chem. Eng. J. 466 (2023) 143173.

[72] R. Luo, J. Dai, J. Zhang, Z. Li, Accelerated skin wound healing by electrical stimulation, Adv. Healthcare Mater. 10 (2021) 2100557.

[73] T. Später, M. Assunção, K.K. Lit, G. Gong, X. Wang, Y.Y. Chen, Y. Rao, Y. Li, C.H. K. Yiu, M.W. Laschke, M.D. Menger, D. Wang, R.S. Tuan, K.H. Khoo, M. Raghunath, J. Guo, A. Blocki, Engineering microparticles based on solidified stem cell secretome with an augmented pro-angiogenic factor portfolio for therapeutic angiogenesis, Bioact. Mater. 17 (2022) 526–541.

[74] Y. Tang, G. Gong, X. He, M. Dai, M. Chen, B. Wang, Y. Wang, X. Wang, J. Guo, Multifunctional dual cross-linked bioadhesive patch with low immunogenic response and wet tissues adhesion, Adv. Healthcare Mater. 12 (2023) 2201578.

[75] J. Mao, L. Chen, Z. Cai, S. Qian, Z. Liu, B. Zhao, Y. Zhang, X. Sun, W. Cui, Advanced biomaterials for regulating polarization of macrophages in wound healing, Adv. Funct. Mater. 32 (2022) 2111003.

[76] L. Mao, S. Hu, Y. Gao, L. Wang, W. Zhao, L. Fu, H. Cheng, L. Xia, S. Xie, W. Ye, Z. Shi, G. Yang, Biodegradable and electroactive regenerated bacterial cellulose/MXene (Ti$_3$C$_2$T$_x$) composite hydrogel as wound dressing for accelerating skin wound healing under electrical stimulation, Adv. Healthcare Mater. 9 (2020) 2000872.

[77] D.Z. Zmejkoski, N.M. Zdravković, D.D. Trišić, M.D. Budimir, Z.M. Marković, N. O. Kozyrovska, B.M. Todorovic Markovic, Chronic wound dressings–pathogenic bacteria anti-biofilm treatment with bacterial cellulose-chitosan polymer or

bacterial cellulose-chitosan dots composite hydrogels, Int. J. Biol. Macromol. 191 (2021) 315–323.

[78] Z. Zhao, D.C. Pan, Q.M. Qi, J. Kim, N. Kapate, T. Sun, C.W.T. Shields, L.L. Wang, D. Wu, C.J. Kwon, W. He, J. Guo, S. Mitragotri, Engineering of living cells with polyphenol-functionalized biologically active nanocomplexes, Adv. Mater. 32 (2020) 2003492.

[79] Y. Ju, H. Liao, J.J. Richardson, J. Guo, F. Caruso, Nanostructured particles assembled from natural building blocks for advanced therapies, Chem. Soc. Rev. 51 (2022) 4287–4336.

[80] A.M. Navara, Y.S. Kim, Y. Xu, C.L. Crafton, M. Diba, J.L. Guo, A.G. Mikos, A dual-gelling poly(*N*-isopropylacrylamide)-based ink and thermoreversible poloxamer support bath for high-resolution bioprinting, Bioact. Mater. 14 (2022) 302–312.

[81] J.C. Bi, S.X. Liu, C.F. Li, J. Li, L.X. Liu, J. Deng, Y.C. Yang, J. Morphology and structure characterization of bacterial celluloses produced by different strains in agitated culture, Appl. Microbiol. 117 (2014) 1305–1311.